Acta Pharmaceutica Sinica B 2024;14(9):3931−3948

Chinese Pharmaceutical Association
Institute of Materia Medica, Chinese Academy of Medical Sciences

Acta Pharmaceutica Sinica B

www.elsevier.com/locate/apsb
www.sciencedirect.com

ORIGINAL ARTICLE

Beyond ribosomal function: RPS6 deficiency suppresses cholangiocarcinoma cell growth by disrupting alternative splicing

Wenkang Fu [a,†], Yanyan Lin [b,†], Mingzhen Bai [a,†], Jia Yao [a,c,*], Chongfei Huang [a], Long Gao [a], Ningning Mi [a], Haidong Ma [a], Liang Tian [a], Ping Yue [b], Yong Zhang [b], Jinduo zhang [b], Yanxian Ren [b], Liyun Ding [d], Lunzhi Dai [e], Joseph W. Leung [f], Jinqiu Yuan [g,*], Wenhua Zhang [h,*], Wenbo Meng [a,b,*]

[a]*The First School of Clinical Medicne, Lanzhou University, Lanzhou 730030, China*
[b]*Department of General Surgery, the First Hospital of Lanzhou University, Lanzhou 730030, China*
[c]*Key Laboratory of Biotherapy and Regenerative Medicine of Gansu Province, the First Hospital of Lanzhou University, Lanzhou 730000, China*
[d]*School of Physical Science and Technology, Lanzhou University, Lanzhou 730000, China*
[e]*National Clinical Research Center for Geriatrics and Department of General Practice, State Key Laboratory of Biotherapy, West China Hospital, Sichuan University, Chengdu 610041, China*
[f]*Division of Gastroenterology, UC Davis Medical Center and Sacramento VA Medical Center, Sacramento, CA 95817, USA*
[g]*Clinical Research Center, Big Data Center, the Seventh Affiliated Hospital, Sun Yat-sen University, Shenzhen 518107, China*
[h]*School of Life Sciences, Lanzhou University, Lanzhou 730000, China*

Received 20 February 2024; received in revised form 5 May 2024; accepted 23 May 2024

KEY WORDS

Cholangiocarcinoma;
Ribosomal protein S6;
Alternative splicing;

Abstract Cholangiocarcinoma (CCA) is a bile duct malignancy with a dismal prognosis. This study systematically investigated the role of the ribosomal protein S6 (*RPS6*) gene, which is dependent in CCA. We found that RPS6 upregulation in CCA tissues was correlated with a poor prognosis. Functional investigations have shown that alterations in RPS6 expression, both gain- and loss-of function could

*Corresponding authors.
E-mail addresses: yaoj06@lzu.edu.cn (Jia Yao), yuanjq5@mail.sysu.edu.cn (Jinqiu Yuan), zwh@lzu.edu.cn (Wenhua Zhang), mengwb@lzu.edu.cn (Wenbo Meng).
[†]These authors made equal contributions to this work.
Peer review under the responsibility of Chinese Pharmaceutical Association and Institute of Materia Medica, Chinese Academy of Medical Sciences.

https://doi.org/10.1016/j.apsb.2024.06.028

p53;
Minichromosome maintenance complex component 7;
Vivo morpholino;
Patient-derived organoids

affect the proliferation of CCA cells. In xenograft tumor models, RPS6 overexpression enhances tumorigenicity, whereas RPS6 silencing reduces it. Integration analysis using RNA-seq and proteomics elucidated downstream signaling pathways of RPS6 depletion by affecting the cell cycle, especially DNA replication. Immunoprecipitation followed by mass spectrometry has identified numerous spliceosome complex proteins associated with RPS6. Transcriptomic profiling revealed that RPS6 affects numerous alternative splicing (AS) events, and combined with RNA immunoprecipitation sequencing, revealed that minichromosome maintenance complex component 7 (*MCM7*) binds to RPS6, which regulates its AS and increases oncogenic activity in CCA. Targeting RPS6 with vivo phosphorodiamidate morpholino oligomer (V-PMO) significantly inhibited the growth of CCA cells, patient-derived organoids, and subcutaneous xenograft tumor. Taken together, the data demonstrate that RPS6 is an oncogenic regulator in CCA and that RPS6-V-PMO could be repositioned as a promising strategy for treating CCA.

1. Introduction

Cholangiocarcinoma (CCA) is a rare but highly malignant tumor that originates from various epithelial cells of the bile duct throughout the biliary tree[1]. This disease accounts for ∼15% of all primary liver tumors and 3% of gastrointestinal cancers, and is the second most prevalent cause of hepatobiliary tumors[2]. Early CCA is asymptomatic, and generally, it is often already advanced by the time patients are diagnosed[3]. Although surgery is the preferred curative strategy for patients with CCA, only ∼25% of patients can undergo for radical surgical resection[4]. Thus, a more comprehensive understanding of the molecular mechanisms regulated by oncogenic drivers in CCA is required, and the identification of novel interventional strategies is critical to improve the survival outcomes of CCA patients.

Multiomics encompasses protein and genomic screening strategies that can elucidate new disease subtypes and pathogenesis, and aid in identifying potential therapeutic targets[5]. Multiomics analyses of clear cell renal cell carcinoma[6], endometrial carcinoma[7] and hepatocellular carcinoma[8,9], as well as colorectal[10] and colon carcinoma[11], have been performed with notable results. This approach might help identify new mechanisms and novel targets to develop more treatment options for patients with CCA. We used proteomics and bioinformatics analysis of established datasets and further investigated RPS6 because of its abundant expression and uncharacterized role in CCA. As a ribosomal RNA-binding protein (RBP), RPS6 belongs to the 40S small ribosomal subunit family that is involved in regulating mRNA translation[12]. Furthermore, in addition to its classic function, RPS6 also has extraribosomal functions and has critical roles in several cellular processes such as cell proliferation, DNA repair, apoptosis, and cellular differentiation[13-15]. In addition, upregulated, and intrinsically dysfunctional ribosomes are involved in tumor development, and RPS6 is often overactivated in numerous types of tumors[16-20]. Herein, we found that RPS6 is frequently upregulated and is associated with the prognosis of patients with CCA.

Altered ribosomal protein (RP) expression impairs ribosome biogenesis, and results in activation of the tumour protein p53 (p53)[21]. However, some RPs may also regulate translation or transcription through biological processes unrelated to p53 outside ribosome[15]. For instance, extraribosomal RPS3 and RPS14 interact with DNA-binding complexes to regulate gene-specific transcription. Similarly, RPL32, RPS13 and RPL22 regulate the expression of target genes during the splicing process[22-24]. In eukaryotes, RNA splicing is a posttranscriptional mechanism that promotes RNA and protein expression[25]. The process of RNA splicing is executed by a substantial ribonucleoprotein (RNP), and the crystal structure of the prototypical RNA domain of U1 small nuclear ribonucleoprotein A (U1A), revealed that RPS6 has essentially the same fold as the U1A protein. Therefore, RPS6 is a candidate RNP protein that can bind to multiple RNAs[26].

We found that elevated RPS6 was associated with a poor prognosis among patients with CCA. Impaired RPS6 expression inhibited CCA tumorigenesis and progression both *in vitro* and *in vivo*. We used RNA sequencing (RNA-seq) and proteomics, to explore the effects of deleting RPS6 on the enrichment of downstream signaling pathways involved in the cell cycle, particularly DNA replication. Alterations of RPS6 expression disrupted ribosome biogenesis, and triggered the activation of p53, which is a typical cell cycle regulatory factor. Mapping of the RPS6 protein interactions *via* immunoprecipitation followed by mass spectrometry (IP-MS) revealed an essential CCA splicing network, and further AS analysis identified multiple RPS6-regulated events, particularly, RPS6 binds and modulates splicing of the *MCM7* mRNA, which is essential for DNA unwinding and cell duplication. Finally, Attenuating RPS6 translation using V-PMO, which significantly inhibits the growth of CCA cells and PDOs. In summary, our findings showed that RPS6 plays pro-tumorigenic functions in the development of CCA *via* synergistic effects on both of inner and outer nuclear pathways, and that therapeutic targeting of RPS6 may provide avenues for the intervention of CCA.

2. Materials and methods

2.1. CCA tissue specimens and cell lines

We obtained ten fresh-frozen CCA and para-tumor samples from surgical resections of CCA patients at the First Hospital of Lanzhou University (Lanzhou, China). These samples were stored at −80 °C after freezing in liquid nitrogen. We used three specimens for mass spectrometry-based proteomic analysis and seven for Western blot analysis. All human samples were collected with

the informed consent of the donors. The Ethics Committee of the First Hospital of Lanzhou University approved this study, and the approval number is LDYYLL2022-452.

Human intrahepatic bile duct epithelial cells (HIBEpiC) were purchased from ICell Bioscience Inc. (Shanghai, China), and cultured in ICell primary epithelial cell culture system medium (ICell Bioscience Inc.). CCA cell lines RBE and HCCC-9810 were purchased from the National Biomedical Experimental Cell Resource Bank (BMCR, Beijing, China); the HuCCT1 cell line was purchased from Shanghai Fuheng Biotechnology Co., Ltd. (Shanghai, China). The TFK-1 cell line was purchased from Creative Bioarray (NY, USA). All these CCA cell lines were cultured in RPMI 1640 (GIBCO, USA) medium, supplemented with 10% fetal bovine serum (Cell-Box Biological Products Trading Co., Ltd., Hong Kong, China), penicillin and streptomycin (GIBCO, USA). The cells were maintained at 37 °C in a 5% CO_2 cell culture incubator. These CCA cell lines were correctly identified by STR analysis by the China Center for Type Culture Collection (CCTCC, Wuhan, China), and HIBEpiC cells were subjected to STR analysis without matching any profile in the ExPASy STR database.

2.2. *Quantitative proteomic analysis*

Proteomic analysis was performed as previously described[27], and an iTRAQ Reagent Kit (Applied Biosystems, CA, USA) and TMT Reagent Kit (Thermo Scientific, IL, USA) were used in this study. Total proteins were extracted from CCA tissues and cells. Fifty microlitres of dissolution buffer and 4 μL of reducing reagent were added to 100 μg of dried protein from each sample, then incubated the solution at 60 °C for 1 h. After alkylating with 2 μL of cysteine blocking reagent, the protein solution was cleaned using 10 kDa ultrafiltration, and the digestion was prepared by addition of 50 μL of sequencing-grade trypsin (Promega, WI, USA) for 12 h at 37 °C. The solution was centrifuged, and the enzymatic peptides were collected. Peptides from six samples were individually labelled with the iTRAQ or TMT tag and then lyophilized for further chromatographic analysis.

Reverse phase liquid chromatography (RPLC)-fractioned samples were subjected to high-performance liquid chromatography (HPLC) on an Agilent 1200 HPLC system (Agilent, CA, USA) and analyzed by tandem mass spectrometry combined with liquid chromatography (LC−MS/MS). Data acquisition was performed with a Triple TOF 5600 System (AB SCIEX, MA, USA) fitted with a Nanospray III source (AB SCIEX) and a pulled quartz tip as the emitter (New Objectives, MA, USA). Finally, the data were processed with Protein Pilot Software v. 5.0 (AB SCIEX) against the Homo Sapiens database using the Paragon algorithm. Differentially expressed proteins (DEPs) were identified with a fold change (FC) > 1.2 or < 0.83 and a P value < 0.05, indicating up- or downregulation in two comparable groups.

2.3. *Lentivirus transfection*

The lentiviral packaging plasmid was from Genechem (Shanghai, China). Two targeted RPS6 knockdown small hairpin RNA (shRNA) sequences—5′-GCTGCAGAATATGCTAAACTT-3′ and 5′-CCGCCAGTATGTTGTAAGAAA-3′—and a negative control (NC) sequence—5′-TTCTCCGAACGTGTCACGT-3′—were used. We performed lentivirus transfection according to the manufacturer's instructions. Stably transfected cells were selected using the antibiotic puromycin at a concentration of 2 μg/mL. Tet-ON controlled transgenes were activated by culturing cells in the presence of 1 μg/mL doxycycline (MCE, Wuhan, China) for 72 h. We counted RBE cells expressing shRPS6 and shNC using a Celigo® Imaging Cytometer (Nexcelom Bioscience, MA, USA).

2.4. *RNA isolation, quantitative real-time PCR (qRT-PCR) and RT-PCR*

According to the manufacturer's instructions, total RNA was isolated from harvested cell lines or tumor tissues using TRIzol reagent (Invitrogen, CA, USA). RNA concentration was measured by spectrophotometer (NanoDrop Technologies Inc., DE, USA). The cDNA synthesis was conducted by using the Reverse Transcription System (TaKara, Dalian, China). The bio-rad real-time PCR instrument (Biorad, CA, USA) was used to evaluate the quantities of RNA transcripts. All PCR reactions were conducted using 2 × Taq PCR MasterMix II (Tiangen, Beijing, China) following the manufacturer's instructions. The primers sequences were listed in Supporting Information Table S1.

2.5. *Western blot analysis*

Total protein was extracted from harvested cell lines or tumor tissues by RIPA lysis buffer with PMSF (ThemoFisher). After centrifuging lysates for 15 min at 12,000 rpm (Micro17R, ThemoFisher Scientific, MA, USA) and 4 °C, the supernatants were collected, and BCA Protein Assay Reagent (Absin, Shanghai, China) was used to measure the protein concentrations. Lysates have been transferred onto PVDF membranes after being size-separated using SDS-PAGE. The membranes were blocked in 5% nonfat milk and then incubated with primary specific antibodies at 4 °C overnight. The dilutions of the primary antibodies were used as follows: anti-RPS6 (1:1000), anti-MDM2 (1:1000), anti-p21 (1:1000), anti-MCM7 (1:1000), anti-CCNB1 (1:1000), which were purchased from CST (Boston, USA); anti-p53 (1:5000), anti-CDK4 (1:4000), anti-CCNA2 (1:5000), anti-MCM6 (1:4000), anti-GAPDH (1:5000), which were purchased from Proteintech (IL, USA); anti-CDK1 (1:1000), anti-CDK2 (1:1000), anti-CDK6 (1:500), anti-MCM2 (1:1000), anti-MCM4 (1:1000), which were purchased from Jingjie PTM BioLab (Hangzhou, China); and anti-SF3B1 (1:1000), which was purchased from Abcam (Cambridge, UK). After three TBST washes, the membrane was incubated with a secondary antibody for 1 h at room temperature, and detected the signals using chemiluminescence.

2.6. *Tissue microarrays (TMAs) and immunohistochemistry (IHC)*

CCA TMAs containing 174 tumor and 117 matched paratumor tissue samples (Shanghai Outdo Biotechnology, Shanghai, China) were used to measure RPS6 expression. TMAs were approved by the Ethics Committee of the Shanghai Outdo Biotechnology. CCA and mouse tumor tissues were deparaffinized and rehydrated after a 2 h incubation at 60 °C, and citrate buffer was used to retrieve antigen. The portions were incubated with 3% hydrogen peroxide at room temperature for 10 min to suppress endogenous peroxidase activity. Afterwards, the slides were incubated with 5% normal goat serum for 30 min at room temperature. The slides were incubated with the specific antibody at 4 °C overnight, Finally, the HRP-labeled secondary antibody was incubated with each slide after washing, and DAB chromogen before hematoxylin counterstaining. The dilutions of the primary antibodies were used

as follows: anti-RPS6 (1:200), anti-ki67 (1:400), anti-MCM7 (1:600), which were purchased from CST (Boston, USA). We analyzed RPS6 staining intensity using Image Pro-Plus and stratified patients into high and low RPS6 expression groups based on the median staining intensity values.

2.7. Cell proliferation and colony formation assay

Cell viability was measured by adding Cell Counting Kit-8 (CCK-8) (Dojindo, Beijing, China) into cell cultured medium in 96-well plates and incubated at 37 °C for 2 h. Cells were plated at a density of 1×10^3 RBE and HuCCT1 cells as well as 3×10^3 TFK-1 cells per well. The proliferation rates were determined at 0, 24, 48, 72 and 96 h, and absorbance detection was performed on a microtiter plate reader set at 450 nm. The numbers presented are the mean ± SD of six data points from a representative experiment. For colony formation assay, 1×10^3 cells were plated in 6-well plates and the medium was refreshed every 3 days. Colonies were fixed with 4% paraformaldehyde after 2 weeks, and stained with 0.1% crystal violet (Solarbio, Beijing, China) for 20 min. At least three experiments were performed.

2.8. Cell cycle and apoptosis analysis

Cell cycle distributions were measured by using Hoechst 33342 (ThemoFisher) in post-transfection cell cultured medium in 6-well plates and incubated at 37 °C for 1 h. Then the cells were detached with TrypLE and washed with PBS. For apoptosis ratio detection assay, the cells were stained by using Annexin V/PI Cell Apoptosis Kit (BD Biosciences, USA) according to the manufacturer's recommendations. Fluorescence was quantified using flow cytometry (Agilent Technologies, Singapore).

2.9. Senescence-associated β-galactosidase (SA-β-gal) staining assessment

A SA-β-gal kit (Beyotime, Shanghai, China) was used for staining senescent cells according to the manufacturer's instructions. Transfected RBE and HuCCT1 from different groups were planted in 6-well plates. After 3 days, cells were fixed for 15 min with fixative solution. The cells were stained by adding 1 mL of staining solution with β-galactosidase and X-Gal at 37 °C overnight after two washes with PBS. The cells that exhibited β-galactosidase activity were classified as senescent cells and were quantified in a minimum of five randomly selected fields.

2.10. Xenograft tumor models

All animal experiments were conducted in accordance with the legal mandates and national guidelines for the care and maintenance of laboratory animals and were approved by the Ethics Committee of the First Hospital of Lanzhou University (LDYYLL2022-452). For tumorigenesis assay, the cells were infected with collected and then resuspended 5×10^6 cells in 100 μL 1:1 mixture 1640 and Matrigel (BD Biosciences, USA) were injected subcutaneously into NOD/SCID mice (Charles River, Beijing, China) at 6−8 weeks old. There were four or six mice in each group. For RPS6 KD tumorigenesis assay, mice in all groups were fed with doxycycline (2000 ppm) containing food and water (containing 2 mg/mL of doxycycline and 5% sucrose) for the whole period. Doxycycline−sucrose solution was provided with fresh preparation every 3−4 days. After 7 days of injection, calipers measured the dimensions of xenografted tumors, and volumes were calculated using Eq. (1) for tumor growth curves:

$$V = 1/2 \times \text{Length} \times \text{Width}^2 \quad (1)$$

After 5 weeks, the mice were sacrificed, and the weights of the xenografts were examined. We examined the expressions of RPS6, Ki-67, and MCM7, in paraffin-embedded tissues.

2.11. RNA-seq

RNA-seq was processed according to the instructions of NEBNextR UltraTM Directional RNA Library Prep Kit for Illumina (NEB, USA). Total RNAs were isolated from RBE cells that were either control or RPS6-depleted with three biological replicates of each strain. mRNA was purified from total RNA using poly-T oligo-attached magnetic beads. cDNA was synthesized using random hexamer primer and M-MuLV Reverse Transcriptase. Then PCR was performed with Phusion High-Fidelity DNA polymerase, Universal PCR primers and Index(X) Primer. At last, PCR products were purified (AM Pure XP system) and library quality was assessed on the Agilent Bioanalyzer 2100 system. After cluster generation, the library preparations were sequenced on an Illumina Hiseq Xten platform and paired-end reads were generated. HISAT2 tools software was used to map the reference genome. Gene expression levels were estimated by fragments per kilobase of transcript per million fragments mapped (FPKM). Genes with an adjusted P-value <0.01 and absolute value of $\log_2(\text{FC}) > 1$ found by DESeq were assigned as differentially expressed.

2.12. Gene ontology (GO), gene set enrichment analysis (GSEA) and kyoto encyclopedia of genes and genomes (KEGG) analysis

The Cluster Profiler R package was employed for GO enrichment analysis on differentially expressed genes (DEGs), utilizing hypergeometric testing to identify significantly enriched GO terms compared to the entire genome background. Additionally, GSEA was performed using Cluster Profiler. KEGG database facilitates understanding of biological functions leveraging molecular-level data from genome sequencing and high-throughput experimental technologies. Statistical enrichment analysis of DEGs in KEGG pathways was conducted using KOBAS software. Cluster Profiler R packages were used to identify significantly enriched KEGG pathways compared to the entire genome background.

2.13. SUnSET assay

SUnSET assays were performed as previously described[28]. The cells were incubated with 1 μmol/L puromycin under normal culture conditions for 30 min. Cell lysates were then collected, and samples were separated by SDS-PAGE. Proteins were transferred to membranes and immunoblotting with anti-puromycin antibody (1:25,000, Sigma−Aldrich, Germany). The blots were visualized using a chemiluminescence imager.

2.14. EdU assay

EdU assay kit (Biyuntian, Shanghai, China) was utilized. Cells were treated with a 10 μmol/L solution of 5-ethynyl-20-

deoxyuridine for 2 h at 37 °C, then fixed with 4% paraformaldehyde for 20 min. Following permeabilization with 0.3% Triton X-100 for 10 min, cells were incubated with Click Additive Solution for 30 min. Subsequently, a 10-min staining with Hoechst was performed, and images were captured using a Nikon inverted fluorescence microscope.

2.15. IP-MS

For the IP assay of RPS6, we followed the instructions of the BeaverBeads™ Protein A (or A/G) Immunoprecipitation Kit (Beaver, Suzhou, China). Cells were lysed in lysis buffer to extract total protein. To 200 μL of lysate, we added 50 μL of Protein A/G agarose beads that had been washed with 200 μL of binding buffer. The mixture was incubated overnight at 4 °C with moderate shaking in the presence of anti-IgG (CST), anti-RPS6 (Abcam), and anti-SF3B1 (MBL). After incubation, the beads were washed with 200 μL of washing buffer and separated using magnetic forces. The immobile protein complex was eluted at 95 °C using 20 μL of 5 × SDS-PAGE loading buffer for 10 min. The eluate was collected for subsequent Western blot analysis.

2.16. AS analysis

The ABLas pipeline was utilized to define and quantify the AS events (ASEs) and regulate AS events (RASEs) observed between the samples. In summary, the detection of ten types of ASEs in ABLas was accomplished by analyzing splice junction reads. These events were exon skipping (ES), alternative 5′ splice site (A5SS), alternative 3′ splice site (A3SS), intron retention (IR), mutually exclusive exons (MXE), mutually exclusive 5′ untranslated regions (5pMXE), mutually exclusive 3′ untranslated regions (3pMXE), cassette exon, A3SS&ES, and A5SS&ES. The significance of the ratio alteration of ASE regulated by RBPs was evaluated using a student's *t*-test. The events that were deemed significant at a *P*-value cutoff corresponding to a false discovery rate cutoff of 5% were classified as RBP regulated ASEs.

2.17. Double immunofluorescence staining

Cells were seeded into confocal dishes and cultured for 2 days. After rinsing twice with PBS, the cells were fixed with 4% paraformaldehyde at 37 °C for 20 min and permeabilized with 0.1% Triton at RT for 10 min. Blocking with 5% BSA for 1 h. The mouse antibody to RPS6 and the rabbit antibody to SF3B1 are incubated together at 4 °C overnight. The dishes were then rinsed three times with PBS and incubated with IgG-Alexa Fluor® Plus 647 secondary antibody and IgG-Alexa Fluor® 488 secondary antibody for 1 h at RT and washed three times, and the nuclear was stained by DAPI. Images were analyzed using confocal microscopy.

2.18. Molecular docking model

RPS6 and SF3B1 protein structures were obtained from RCSB PDB. Schrödinger's Protein Preparation Wizard module was used for preprocessing, ligand state regeneration, H-bond optimization, energy minimization, and water removal. Protein−protein interaction simulations employed 70,000 ligand rotations and returned 30 poses. Lower interaction scores indicated stronger binding. Protein interaction analysis identified RPS6 binding regions on SF3B1. Complexes were color-labeled, and 3D surface display was utilized.

2.19. RNA immunoprecipitation and high-throughput sequencing (RIP-seq)

Following a single 400 mJ/cm^2 irradiation, RBE cells were lysed in ice-cold wash buffer containing 1 × PBS, 0.1% SDS, 0.5% NP-40, and 0.5% sodium deoxycholate, supplemented with 200 U/mL Takara RNase inhibitor and Roche protease inhibitor cocktail. After 30 min of ice incubation, the lysate was centrifuged at 10,000 rpm (5425R, Eppendorf, Hamburg, Germany) for 10 min at 4 °C. RQ I enzyme (Promega) was added to reach a final concentration of 1 U/μL, followed by incubation at 37 °C for 30 min. DNase activity was halted with stop solution. Supernatant was then subjected to MNase digestion. For immunoprecipitation, supernatant was incubated overnight at 4 °C with RPS6 antibody (Proteintech) and control IgG-antibody (CST), followed by 2-h incubation with protein A/G Dynabeads (Thermo Scientific). Beads were washed with lysis buffer, high-salt buffer, and wash buffers. After elution, RNA was purified using Trizol reagent, and cDNA libraries were prepared using KAPA RNA Hyper Prep Kit. Libraries underwent Illumina NovaSeq 150 nt paired-end sequencing. The ABLIRC method was used to identify RPS6 genome binding sites, with peak analysis performed to identify IP target genes and HOMER software used for protein binding motifs.

2.20. Depletion of RPS6 with an antisense morpholino

Antisense morpholinos were designed to specifically target the translation initiation in the RPS6 transcript (RPS6-V-PMO—TCTTGAAGCAGCTGAACGCCTCCGA). The morpholinos were obtained from GeneTools (USA). A nontargeting morpholino (NT PMO) was employed as a control. For the depletion of RPS6 in the RBE and TFK-1 cells, the growth media was supplied with RPS6 PMO or NT PMO at concentrations ranging from 1 to 10 μmol/L for 48 h. The PDOs were treated with RPS6-V-PMO or NT PMO at concentrations ranging from 1 to 4 μmol/L for 72 h. V-PMO were either intratumorally injected 10−40 μL in xenograft tumor models.

2.21. CCA patients derived organoid (PDOs) culture

Tissue samples were washed in cold 1640 medium with penicillin/streptomycin, followed by two rinses with cold PBS. Subsequent incubation in 4 mmol/L EDTA/PBS solution for 30 min facilitated tumor cell release through forceful pipetting at 10-min intervals. After sedimentation, the supernatant containing tumor cells was collected and mixed with 20 mL cold washing solution before centrifugation. The cell pellet underwent two cold washing rounds and was then resuspended in 75% Matrigel solution. Matrigel domes were incubated at 37 °C for 30 min before adding complete CCA PDO media, organoid passaging utilized mechanical force, and master aliquots were cryopreserved for samples with low passage numbers. Cells were cultured for up to 10 passages before replacement with cells from frozen stocks.

2.22. siRNA and plasmid

Lipofectamine 3000 (Invitrogen) was used to transfect siRNA and plasmid into RBE cells following the manufacturer's instructions[29].

MCM7 siRNAs were from Tsingke Biotech (Beijing, China). Plasmids containing cDNA of MCM7-FL and MCM7-ND were employed to generate exogenous MCM7 isoforms. Cells were harvested for subsequent analysis after 48 h.

2.23. Statistics

The *in vitro* experiments were conducted independently and repeated three times. The statistical analyses were conducted using GraphPad Prism 9.0 (GraphPad Software Inc., CA, USA). The data are presented as mean ± standard deviation (SD), statistical differences were analyzed using the unpaired two-tailed Student's. The Kaplan−Meier method and the log-rank test were used to estimate the overall survival rate. When the P value < 0.05, the obtained results were considered statistically significant. P values are shown and indicated on plots in means of follows ($^{*}P < 0.05$, $^{**}P < 0.01$; $^{***}P < 0.001$, $^{****}P < 0.0001$).

3. Results

3.1. Multiomics screening reveals RPS6 dependency in CCA

Proteomics is essential for the early diagnosis, prognosis and monitoring of disease development. Based on the proteomic findings from iTRAQ screens, we identified 487 DEPs in CCA and pericarcinomatous tissues. The DEPs comprised 234 and 253 upregulated and downregulated proteins, respectively (Fig. 1A). To more comprehensively and accurately assess the expression of these proteins, we systematically investigated the mRNA expression profiles in the TCGA CCA cohort, and approximately 58% (282/487) of the DEPs were also identified as DEGs (Supporting Information Fig. S1A and S1B). According to KEGG pathway analyses, of the differentially expressed molecules (DEMs), both DEPs and DEGs were enriched in the complement and coagulation cascades, ECM-receptor interaction, focal adhesion, proteoglycans in cancer, PI3K−Akt signaling pathway, spliceosome, and these signaling pathways are linked to the metastasis and proliferation of CCAs (Fig. 1B). Subsequently, we assessed the dependence of these DEMs on CCA progression using the DepMap portal (https://depmap.org/portal/), and found that 13 DEMs were dependent on RBE and TFK-1 CCA cell lines (Fig. 1C and D, Fig. S1C). We excluded some dependent genes that are also considered core fitness genes[30], to augment the significance of the targeted treatment and RPS6, which was the most dependent, for further exploration (Fig. 1E, Fig. S1D). Using Celigo cell cycle proliferation analysis, we further confirmed that RPS6 plays a critical role in the growth of CCA cells. The results showed that RPS6 knockdown significantly inhibited RBE cell proliferation. Changes in proliferation on the fifth day were 2.28-fold higher than that on the first day in the RPS6 KD group, whereas proliferation in the control group increased 7.75-fold (Fig. 1F and G, Fig. S1E and S1F). Moreover, the sequencing data from the TCGA database were integrated with the IHC results obtained from the Human Protein Atlas portal (https://www.proteinatlas.org/). The RPS6 mRNA and protein levels were substantially elevated in CCA tissues (Fig. S1G and S1H). Overall, these results indicate that RPS6 upregulation plays a dependent role in CCA growth.

3.2. RPS6 is increased in patients with CCA and associated with CCA prognosis

To determine the clinical importance of RPS6 in CCA. We found that RPS6 protein level exhibited higher expression in CCA tissues (Fig. 2A, Supporting Information Fig. S2A). In addition, we investigated the expression profiles of RPS6 in a panel of CCA cell lines, and observed lower expression of RPS6 in HIBEpic and higher expression of RPS6 in CCA cell lines (Fig. 2B and C, Fig. S2B). Furthermore, IHC staining of TMA to determine RPS6 protein levels revealed stronger staining intensity in CCA, than in para-tumor tissues (Fig. 2D and E). Our clinicopathological correlation analysis indicated a strong association between elevated RPS6 expression and tumor TNM-stage (Fig. 2F−H). Furthermore, we investigated the correlation between RPS6 expression and prognosis in patients with CCA using Kaplan−Meier survival analysis. Elevated RPS6 expression was significantly correlated with reduced overall survival in patients with CCA (Fig. 2I). In summary, these results suggest that RPS6 is overexpressed and is correlated with a poor prognosis for patients with CCA.

3.3. RPS6 deficiency inhibits cell proliferation and tumorigenesis of CCA cells in vitro and in vivo

We examined the modified cellular phenotypes of RPS6-depleted CCA cells and verified the importance of these clinical findings. We stably silenced RPS6 in CCA cells using shRNA-encoding lentiviruses, and confirmed the knockdown efficacy (Fig. 3A, Fig. S2C and S2D). The results of the CCK-8 assays showed that RPS6 knockdown decreased cell proliferation (Fig. 3B). This result was further supported by the colony formation assay, which showed that RPS6 knockdown significantly repressed the colony formation ability of RBE cells (Fig. 3C, Fig. S2F). We conducted a gain-of-function study to examine the impact of RPS6 overexpression on the progression of CCA. We established CCA cells stably overexpressing of RPS6 (Fig. 3D, Fig. S2E) and observed that this overexpression led to increased cell proliferation (Fig. 3E) and colony formation (Fig. 3F, Fig. S2I). We evaluated cell cycle distribution and apoptosis using flow cytometry to determine the mechanism underlying the RPS6-mediated proliferative effect in CCA cells. Knockdown of RPS6 in CCA cells disrupted cell cycle progression through G1 arrest and reduced the number of cells in the S phase, while overexpression of RPS6 can promote cells from G1 phase to S phase (Fig. 3I and J, Fig. S2K and S2L). EdU staining revealed a significant reduction in DNA replication in CCA cells following the silencing of RPS6 (Fig. 3K, Fig. S2M and S2N). Moreover, flow cytometry showed that the apoptosis rate in the RBE cells with silenced RPS6 tended to increase compared to the control group, but the differences were not significant (Fig. S2J and S2K). Collectively, these results suggest RPS6 downregulation predominantly induced cell cycle arrest at the G0−G1 phase but did not promote cell apoptosis. Senescence is generally associated with cellular proliferative capacity and senescent cells are associated with growth arrest, with a particular focus on cells that stop dividing[31]. More RPS6-silenced RBE and HuCCT1 cells stained positive for SA-β-gal compared with their respective controls, and the number of senescent cells was not significantly altered in the RPS6-overexpressing group (Fig. 3G and H, Fig. S2G and S2H). Finally, we evaluated the oncogenic role of RPS6 in CCA *in vivo* using mouse models of subcutaneous tumorigenesis. We subcutaneously injected RPS6 deficient HuCCT1, RPS6-overexpression TFK-1 and control cells were into NOD/SCID mice, respectively.

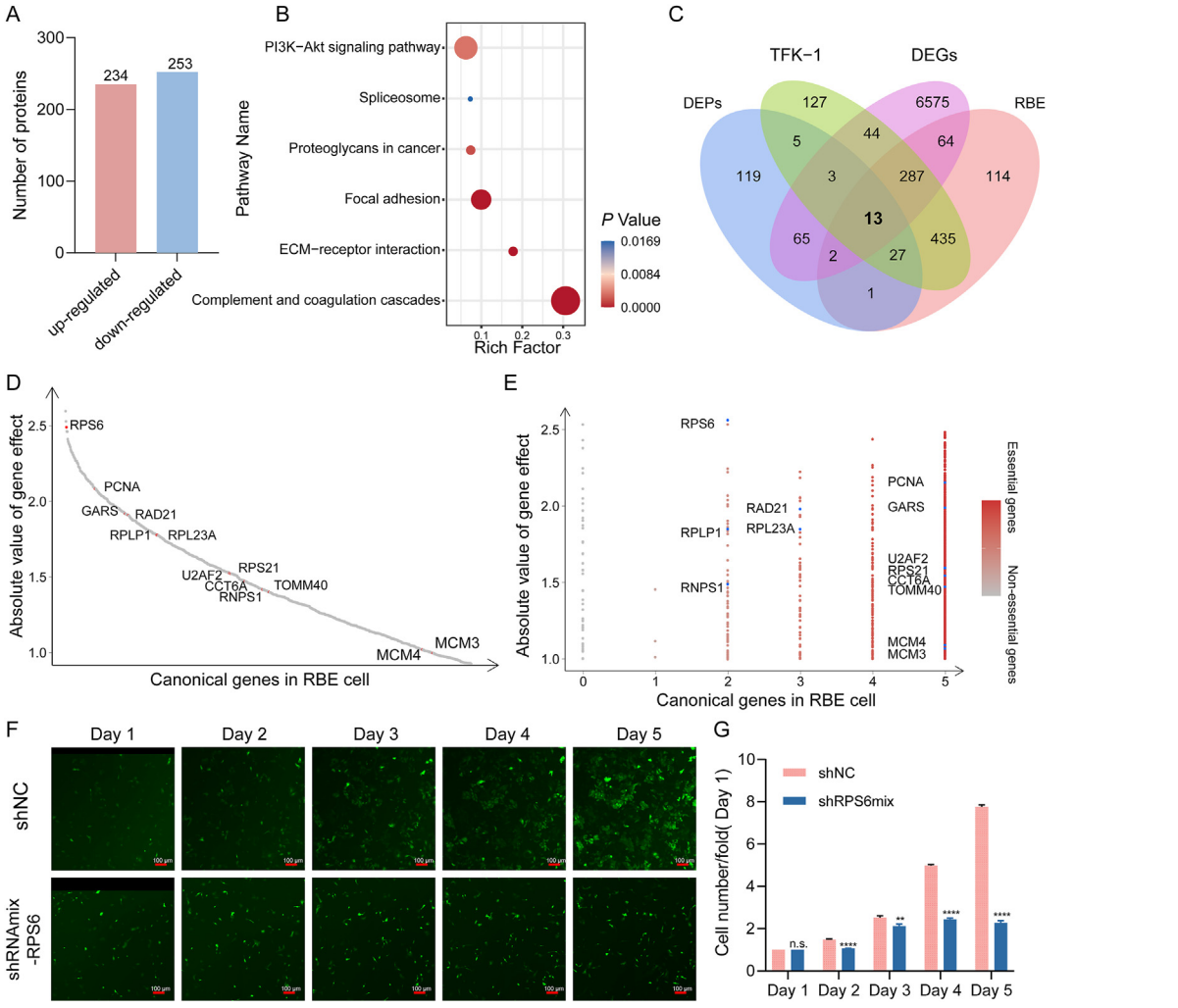

Figure 1 Dependence of RPS6 in CCA by multiomics and functional screening. (A) DEP numbers identified by iTRAQ-based proteomic analysis. (B) KEGG pathway analysis for all DEMs. (C) Overlapping analysis of DEGs, DEPs, RBE and TFK-1 cells dependency genes. (D) Canonical genes with gene effects (absolute value $>$ 1) in RBE cells; the red dots represent the 13 genes. (E) Analysis of genes essentiality in DepMap screens of RBE cells, *X*-axis represents number of cells line (essential gene $>$2 cell lines). Blue dots represent 13 genes. (F) Representative images taken by Celigo imaging cytometer, scale bar: 100 μm. (G) FC in cell number compared to Day 1 in two groups ($n = 3$). Data are shown as mean ± SD. ns: not significant; $^{**}P < 0.01$; $^{****}P < 0.0001$.

After 4−5 weeks, the mice were sacrificed and the tumors were isolated (Fig. 3L). The tumors derived from the RPS6-deficient groups were substantially smaller than those from the control group, while overexpression group displayed larger (Fig. 3M and P). Meanwhile, the average tumor volume and weight at sacrifice were markedly decreased in mice with RPS6 knockdown compared with the control mice, and the results of the RPS6 overexpression group were opposite (Fig. 3N−R). Follow-up IHC analysis of RPS6 in xenografted tissues confirmed that RPS6 effectively decreased cell proliferation *in vivo*. Compared with the control tumors, the RPS6-silenced tumors exhibited decreased RPS6 and Ki-67 signals (Fig. 3S, Fig. S2O). These results demonstrated that loss of RPS6 inhibited CCA tumorigenesis both *in vitro* and *in vivo*.

3.4. Global landscape of protein and gene expression in CCA altered by RPS6

We assessed changes in mRNA and protein expression after RPS6 knockdown using RNA-seq and TMT-labeled proteomics to determine the underlying mechanisms of RPS6 involvement in CCA tumorigenicity (Fig. 4A). First, we performed RNA-seq analysis of RBE cells with RPS6 knockdown. A principal component analysis (PCA) biplot reveals the two groups had distinct distribution patterns and were readily discernible (Fig. S3A). RPS6 depletion resulted in the alteration of 1088 genes globally, including 362 upregulated genes and 729 downregulated genes. Volcano plot analysis revealed that RPS6 was the top significantly downregulated gene (Fig. 4B, Fig. S3B). GO analysis showed that several enriched biological process such as DNA replication, chromosome segregation, mitosis, DNA strand elongation involved in DNA replication, mitotic cell cycle, G2/M transition of mitotic cell cycle, G1/S transition of mitotic cell cycle and DNA repair (Fig. 4C), and the significantly enriched GO terms for cellular component and molecular function were MCM complex and DNA helicase activity (Fig. S3C and S3D). Additionally, GSEA demonstrated that genes altered by RPS6 were associated with cell cycle and DNA replication (Fig. 4D and E). Consistent with RNA-seq showing the effects of genetic

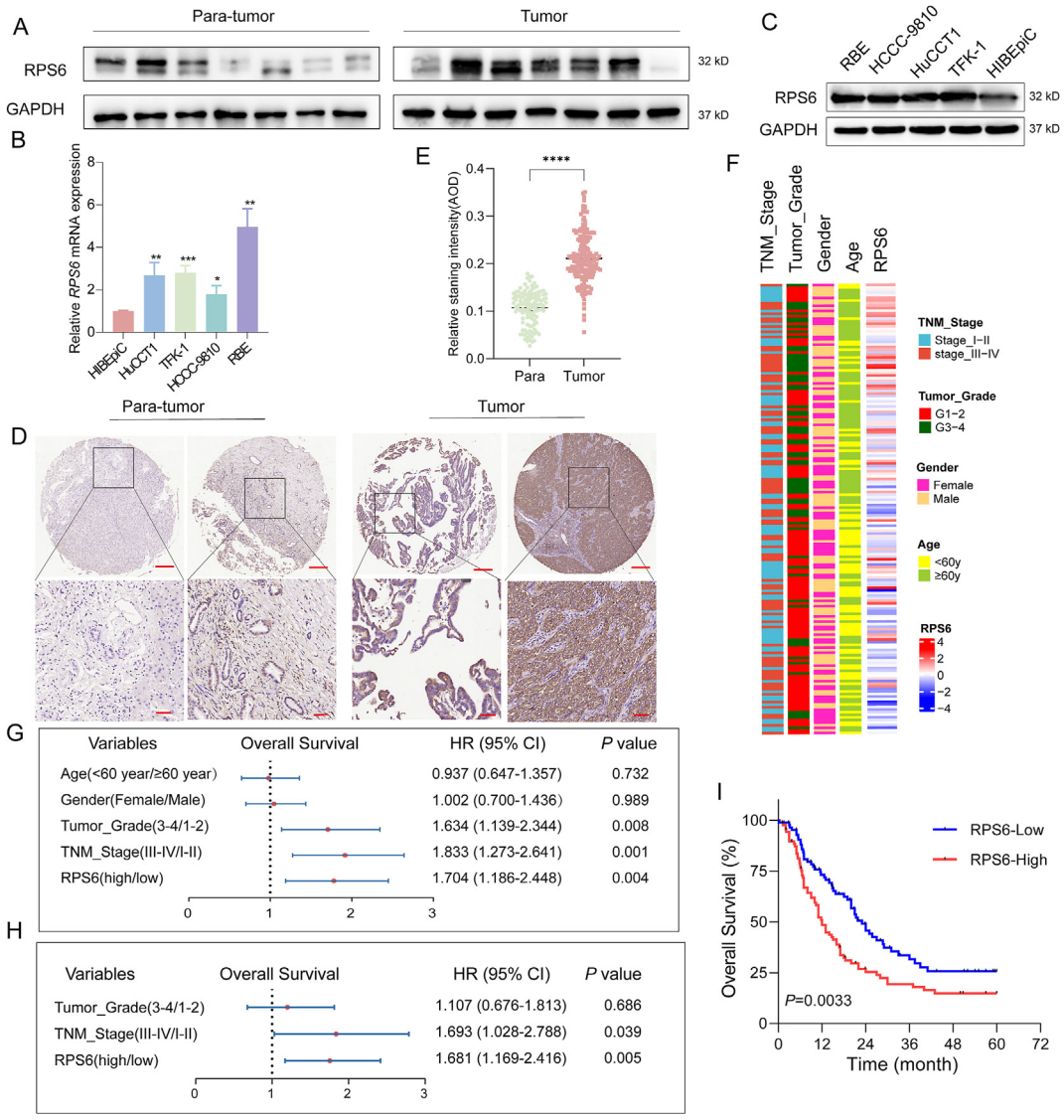

Figure 2 RPS6 expression is elevated in CCA and is associated with a poor patient prognosis. (A) Western blot assays confirmed the upregulation of RPS6 in CCA tissues ($n = 7$), compared to para-tumor tissue ($n = 7$). (B, C) RPS6 mRNA and protein levels in CCA cell lines and HIBEpiC cells. (D) Representative IHC images of RPS6 staining in para-tumor and CCA tissues. Scale bar: 250 μm (upper); Scale bar: 50 μm (below). (E) IHC staining intensities for RPS6 in CCA tissues ($n = 174$) and para-tumor tissue ($n = 117$) from the TMAs. (F) Heatmap showing the RPS6 protein levels and the clinical characteristics of CCA patients from tissue microarrays. (G, H) Univariate & multivariate cox regression analyses showing hazard ratios for overall survival. (I) Kaplan−Meier curves showing the overall survival of 174 CCA patients. Data are shown as mean ± SD. $^{*}P < 0.05$; $^{**}P < 0.01$; $^{***}P < 0.001$; $^{****}P < 0.0001$.

alterations on cell cycle progression, RPS6 knockdown in RBE cells reduced the expression of genes required for DNA replication and cell-cycle progression, including *MCM2, MCM4, MCM6, MCM7, UBC, CDK1, CDK2, CHEK1, CCNA2* and *BUB1B* (Fig. 4F, Fig. S3E). In combination with transcriptional control, protein expression plays a crucial role in the regulation of cellular biological processes. Initially, RPS6 was recognized as the primary substrate of S6K and was hypothesized to function as its effector in the stimulation of protein synthesis[32]. Thus, we applied TMT labeled proteomics analysis to examine global protein abundance changes in RPS6 KD in RBE cells. The PCA biplot reveals the two groups had distinct distribution patterns and were readily discernible (Fig. S3F), For the identification of DEPs we used an absolute threshold for FC ≥ 1.2 with a *P*-value <0.05 and found that compared to those in the RBE NC cells, RPS6 depletion resulted in the alteration of 920 proteins globally, including 488 upregulated proteins and 452 downregulated proteins (Fig. 4G, Fig. S3G). GO analysis revealed several terms such as nucleic acid binding, RNA binding, nuclear division. mitotic nuclear division and ribosomal subunit biogenesis (Fig. S3H). According to KEGG pathway analyses, these DEPs were enriched in the ribosome, DNA replication, cell cycle and p53 signaling pathway (Fig. 4H). Subsequently, we investigated whether the disparate regulation of RNAs was manifested at the protein level. Unexpectedly, we found that only approximately 10% of transcriptional changes were reflected in corresponding changes at the protein level, and most proteome changes were not caused by transcriptional changes (Fig. S3I). The results of the correlation

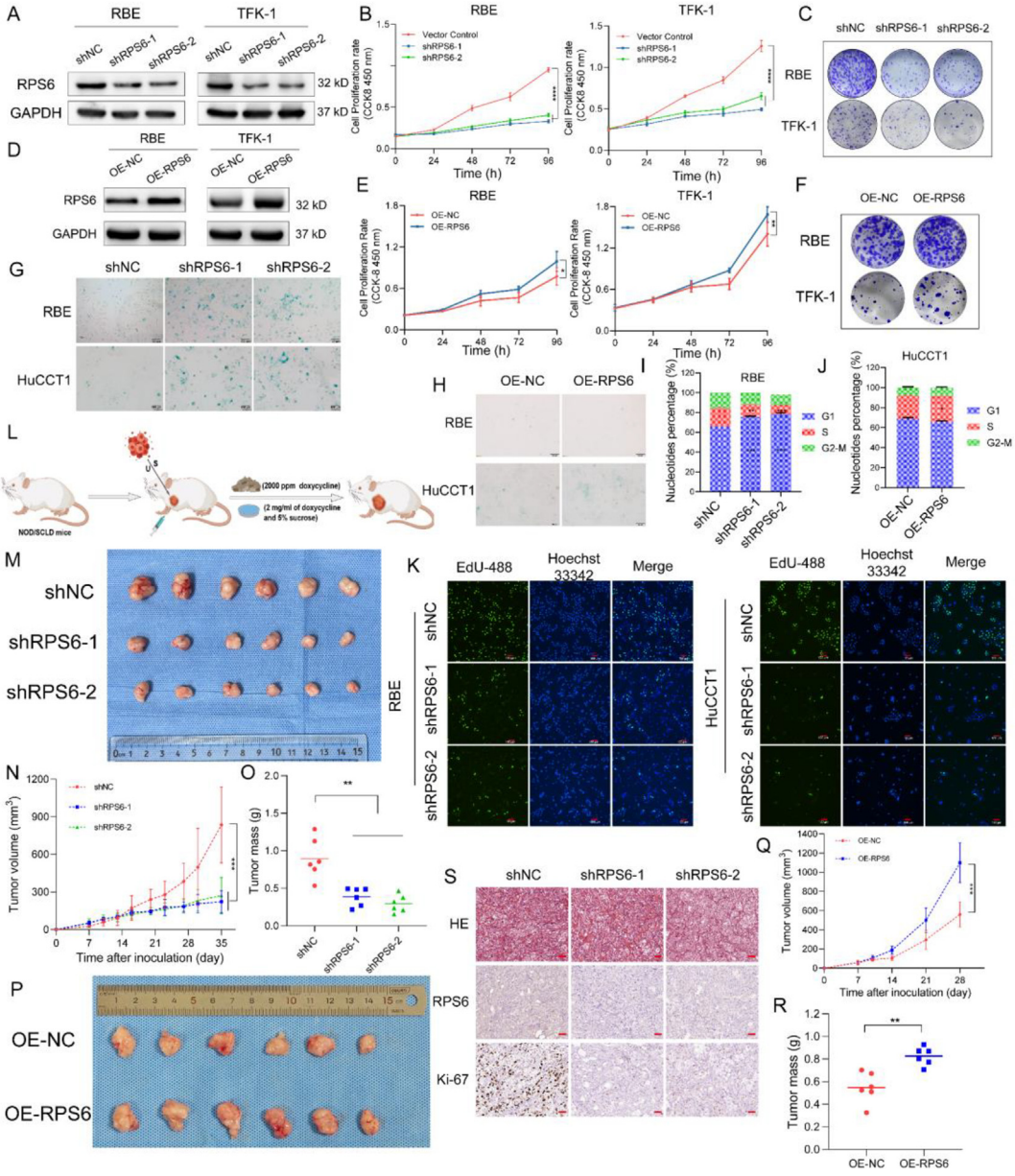

Figure 3 Inhibition of RPS6 suppresses cell growth and tumorigenesis *in vitro* and *in vivo*. (A) Western blot analysis of RPS6 expression in RBE and TFK-1 cells infected two RPS6 shRNAs or a control shRNA. (B, C) CCK-8 ($n = 6$) and colony formation assays were performed to determine cell growth after RPS6 was knocked down in RBE and TFK-1 cells. (D)Western blot analysis for RPS6 expression in RBE and TFK-1 cells infected with the lentiviral empty vector or the RPS6 overexpression lentiviral vector. (E, F) CCK-8 ($n = 6$) and colony formation assays were performed to determine cell growth after RPS6 was overexpressed in RBE and TFK-1 cells. (G, H) Senescent cells were determined by SA-β-gal activity in RBE and HuCCT1 cells. (I, J) Cell cycle distribution ratio in RBE cells after RPS6 knockdown or overexpression ($n = 3$). (K) Results from the EdU incorporation assays of RPS6 knockdown RBE and HuCCT1 cells. Scale bar: 100 μm. (L) Schematics showing the process of the *in vivo* tumorigenesis assay. (M, P) The resected subcutaneous tumors from the three groups are depicted in the image. (N−R) Tumor volumes and mass were calculated ($n = 6$). (S) Representative HE and IHC results. Scale bar: 50 μm. Data are shown as mean ± SD. $^{*}P < 0.05$; $^{**}P < 0.01$; $^{***}P < 0.001$; $^{****}P < 0.0001$.

study indicated a weak significant association between alterations in RNA levels and protein levels (Fig. 4I). However, KEGG pathway analysis showed enrichment of these DEMs in cell cycle, DNA replication, pyrimidine metabolism and p53 signaling pathway (Fig. 4J). These results are consistent with our findings in the previous section on the effects of knocking down RPS6 on CCA cells. In summary, transcript and proteomics analyses delivered large and significant alterations in both the RNA and protein levels following RPS6 KD in RBE cells.

3.5. *RPS6 knockdown induced p53-dependent cell cycle arrest*

Given that RPS6 is an RP, we investigated whether its absence affected other RPs involved in the assembly of the 40S and 60S

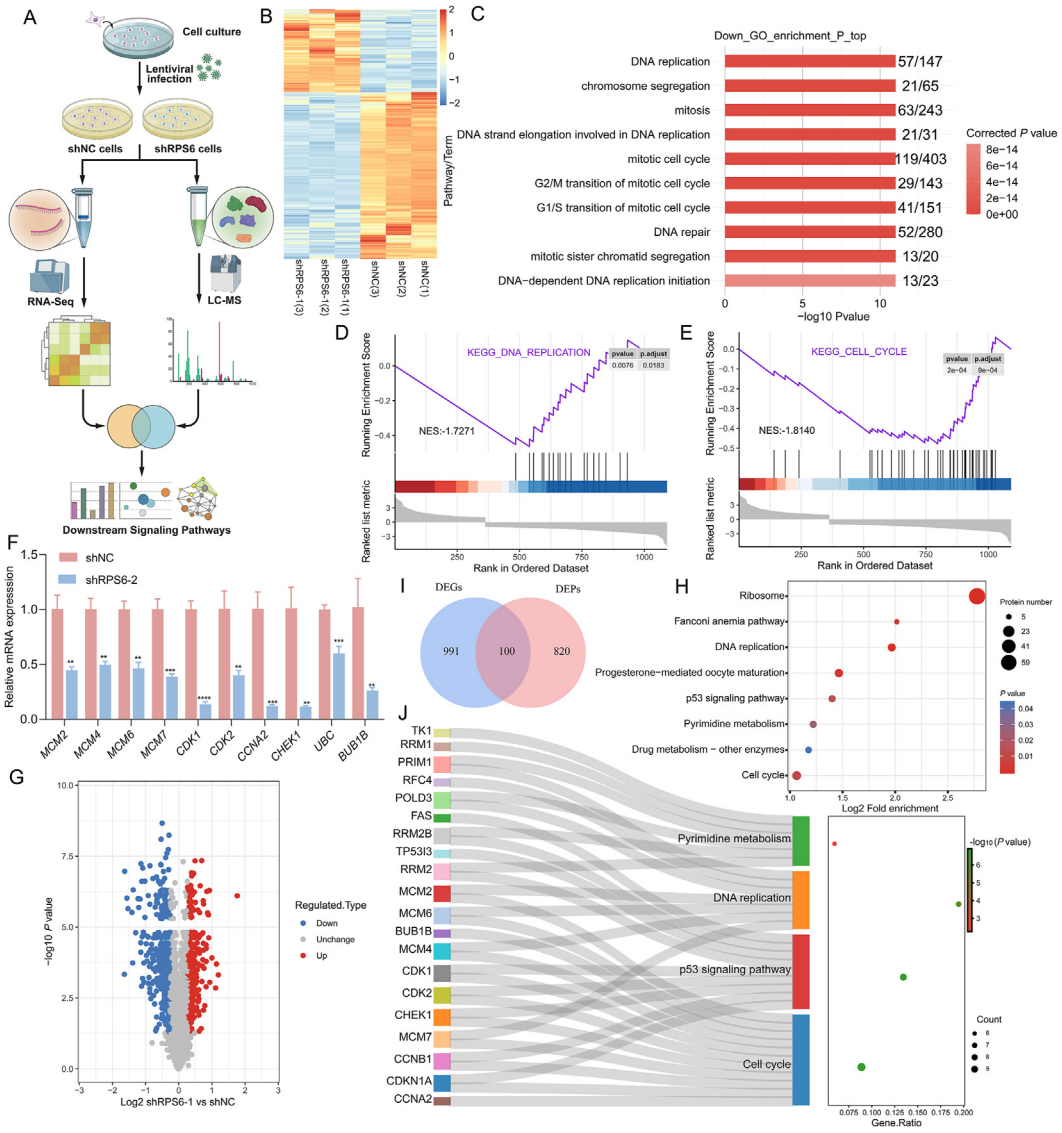

Figure 4 Identification of the underlying mechanism of RPS6 knockdown. (A) Diagram showing the approach used for RNA-seq and TMT-proteomics. (B) Heatmap of DEGs identified by RNA-seq. (C) GO-BP enrichment analysis of DEGs. (D, E) GSEA plots showing the pathways of DEGs altered by RPS6 involved in cell cycle and DNA replication. (F) Validation of cell cycle and DNA replication DEGs mRNA levels ($n = 3$). (G) Volcano plot of DEPs identified by TMT-proteomic. (H) KEGG enrichment analysis of DEPs. (I) Overlapping analysis of DEMs. (J) KEGG enrichment analysis of DEMs. Data are shown as mean ± SD. $^{**}P < 0.01$; $^{***}P < 0.001$; $^{****}P < 0.0001$.

ribosomal subunits. Our proteomics analysis revealed that the RPS6 knockdown group had lower expression levels of the component proteins of both ribosomal subunit (Fig. 5A and B). Then, we investigated the impact of RPS6 on the global protein synthesis rate in CCA cells through SUnSET tests, and the findings indicated that a decrease in RPS6 led to a widespread impairment of protein translation (Fig. 5C−E). Numerous previous studies have provided compelling evidence to support the concept that disruption of ribosome biogenesis leads to the activation of the tumor suppressor protein p53. This activation occurs through the binding of various ribosomal components to its negative regulator MDM2[33] (Fig. 5F). To this end, we first performed gene and protein expression profile analyses in RBE cells with RRS6 knockdown, The KEGG pathway enrichment results that the DEPs were enriched in p53 signal pathway (Fig. 4H). Subsequently, the impact of RRS6 on the protein expression of p53 was assessed. Knockdown of RRS6 resulted in an increase of p53 protein in RBE and HuCCT1 cells. The cell cycle arrest-modulating protein p21 and E3 ubiquitin ligase MDM2, which are downstream targets of p53, were also found to be upregulated (Fig. 5G). The p53 protein functions as a crucial checkpoint in the regulation of the cell cycle, while cell cycle progression is driven by the direct involvement of certain subsets of CDK−Cyclins complexes[34,35]. In line with the findings through proteomics, knockdown of RRS6 led to a decrease of CDKs and cyclins protein levels (Fig. 5H and I). These findings indicate that the depletion of RPS6 triggers p53-mediated cell cycle arrest.

3.6. Downregulation of RPS6 impedes DNA replication by suppression of MCM complex expression

Given the findings from our transcriptional proteomics analyses showing that downstream differential molecules were also enriched in the DNA replication signaling pathway, GO analyses

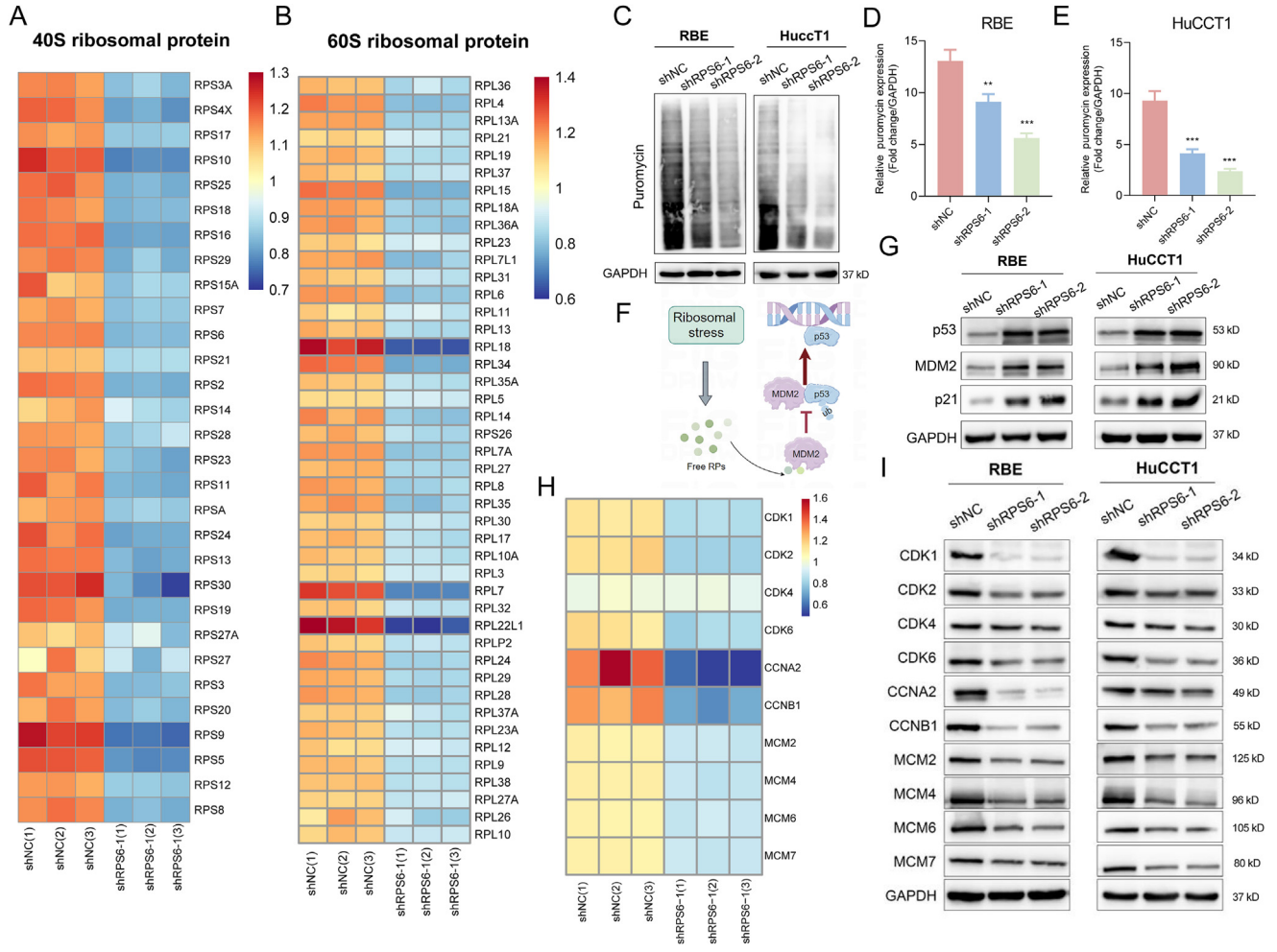

Figure 5 Knockdown of RPS6 induces p53 activation and inhibits DNA replication. (A, B) Heatmap of RP alteration of 40S and 60S identified by TMT-proteomics. (C−E) SUnSET assays to measure the overall rate of novel protein synthesis in RBE and HuCCT1 cells ($n = 3$). (F) Schematic diagram of RP−MDM2−p53 signaling pathway. (G) p53, MDM2 and p21 expression was evaluated in the absence of RPS6. (H) Heatmap of differentially expressed cell cycle and DNA replication proteins levels. (I) Validation of protein levels in H using Western blot. Data are shown as mean ± SD. $^{**}P < 0.01$; $^{***}P < 0.001$.

revealed enrichment of genes related to the MCM complex and DNA helicase activity. In eukaryotes, the MCM complex functions as the replicative helicase, serving as the molecular motor responsible for unwinding duplex DNA and facilitating the advancement of the replication fork during the process of DNA replication[36]. Hence, we also investigated the protein expression of MCM complex components, and the results showed the expression of MCM2, MCM4, MCM6, and MCM7, were also suppressed by RRS6 knockdown (Fig. 5H and I). Additionally, EdU staining demonstrated a notable decrease in DNA replication in CCA cells upon RPS6 silencing (Fig. 3K). Take together, these results indicate that RPS6 potentially modulate DNA replication by regulating the MCM complex.

3.7. Mapping of the RPS6 proteome identifies a splicing network

Using IP-MS, we examined the fundamental mechanism and cofactors associated with RPS6 (Fig. 6A). A comprehensive set of 233 proteins that interact with RPS6 were identified (Fig. 6B). Proteomic network analysis revealed proteins that are closely linked to the spliceosome complex, ribosome biogenesis and mRNA surveillance pathway (Supporting Information Fig. S4A). Since spliceosome complex function during the splicing of pre-mRNAs in the nucleus[37], and our aforementioned results demonstrated that RPS6 may play a role in the nucleus, among the proteins identified by MS, we focused on the higher abundance of SF3B1. To validate the interaction between RPS6 and SF3B1, the association between endogenous RPS6 and SF3B1 was validated with co-IP assays in HuCCT1 and RBE cells (Fig. 6C, Fig. S4B). For a more precise subcellular localization of the RPS6 and SF3B1 proteins, Immunofluorescent double staining experiments demonstrated the colocalization of RPS6 with SF3B1 in the nucleus (Fig. 6E). Additionally, the binding of RPS6 to SF3B1 was predicted using a molecular docking model. The results showed that RPS6 and SF3B1 can bind to each other (Fig. 6D). Together, these data place RPS6 in an extended splicing network that is critical for CCA progression. Next, we further analyzed the

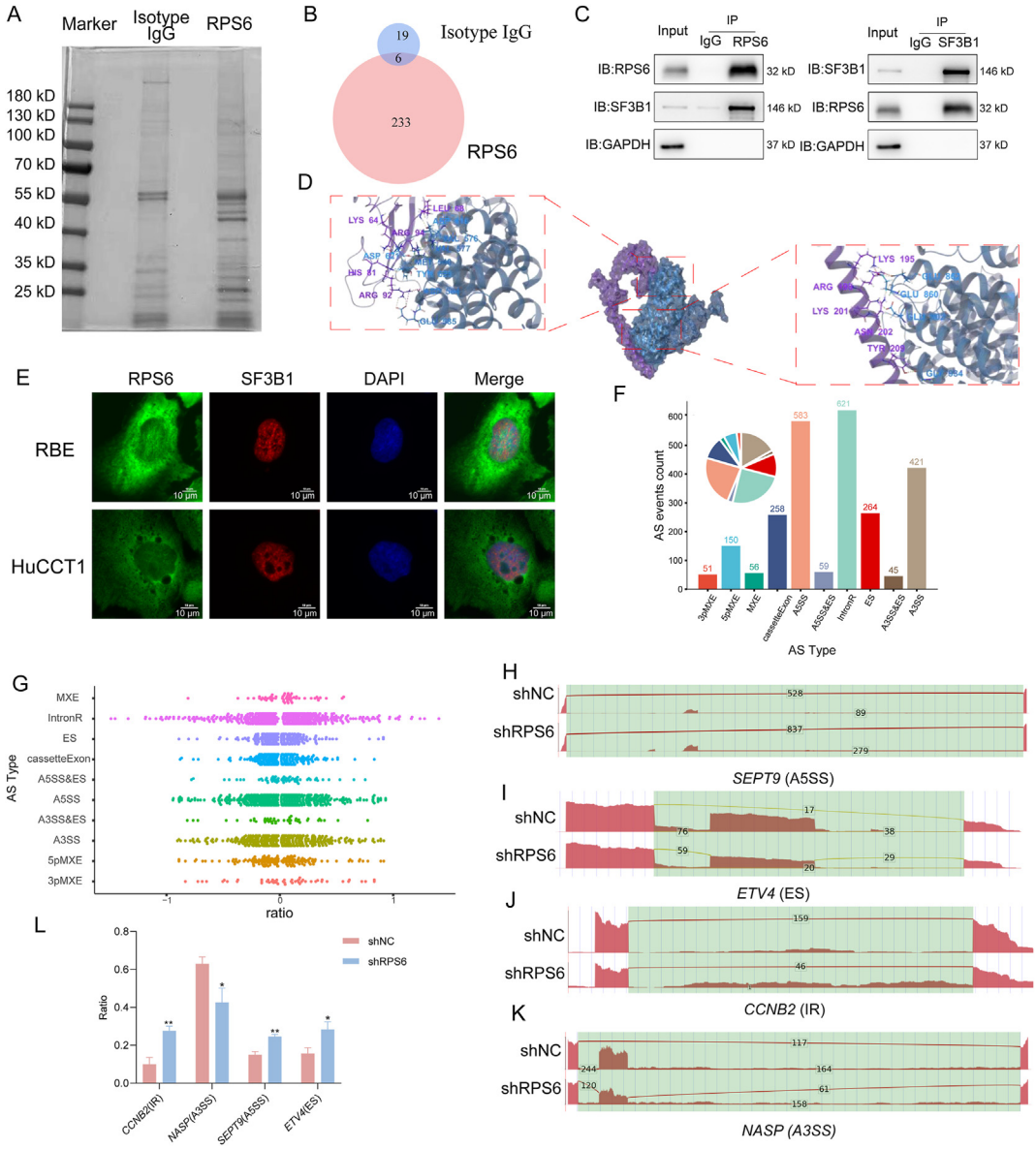

Figure 6 RPS6 loss alters the splicing of mRNAs. (A) IP assay of endogenous RPS6 in RBE cells. (B) Overlay of protein between IgG control and RPS6 IP. (C) Co-IP-WB assay of RPS6 and SF3B1 in HuCCT1 cells. (D) Molecular docking model of RPS6 (blue) interacting with SF3B1 (purple). (E) Immunofluorescence double staining analysis images showing the localization of RPS6 and SF3B1 in RBE and HuCCT1. Scale bar: 10 μm. (F) The type and count of AS events regulated by RPS6. (G) Changes in AS ratio of RPS6-regulated AS events in each category. (H−L) Representative RPS6-affected IR, ES, A3SS and A5SS events and RNA-seq quantification of ASEs ($n = 3$). Data are shown as mean ± SD. *$P < 0.05$; **$P < 0.01$.

AS events induced by knockdown of RPS6 by RNA-seq data. The ASEs and RASEs between the samples were defined and quantified by using the ABLas pipeline as described previously[38,39]. We identified 2508 RASEs, including 51 3pMXE, 150 5pMXE, 421 A3SS, 45 A3SS&ES, 583 A5SS, 59 A5SS&ES, 264 ES, 621 IR, 56 MXE and 258 cassette Exon (Fig. 6F and G). We selected a representative gene in each of the 10 RASGs (Fig. 6H−L and Fig. S4D and S4E). GO analysis of RASGs revealed that RPS6 loss was strongly enriched in processes related to RNA processing, as well as regulation of cell proliferation (Fig. S4C). In summary, these RASGs could either be indirect effects following RPS6-KD induced spliceosome disruption or be directly regulated by RPS6 on targeted transcripts.

3.8. Extra-ribosomal RPS6 regulates CCA carcinogenesis primarily through modulating MCM7 mRNA splicing

RPs are the most abundant type of intracellular RBP and the structure of RPS6 notably resembles a widely recognized RNP that interacts with RNA[40,41]. The effects of RPS6−RNA interactions on pre-mRNA splicing in the context of cancer remains unclear. Thus, in this study, we conducted RIP-seq analysis with the RBE cells to elucidate the genome-wide RNA targets of RPS6. Sample correlation analysis showed a weak correlation between the RIP sample and the input sample, suggesting that the distribution of most reads on the chromosome differed in the two samples, implying a higher degree of enrichment and specificity of

RPS6-bound RNA (Fig. 7A). We observed that the binding regions of RPS6 on genome were most abundant in protein coding sequence (CDS) region of transcripts (Fig. 7B). We identified 8719 IP peaks that were shared between the two groups (Supporting Information Fig. S5A), and RPS6 preferred to bind with a predominant enrichment motif of the AUGGA sequence (Fig. 7C). The identification of target genes of IP was ultimately accomplished by analyzing the peaks, and two representative gene binding peaks are shown in Fig. S5B and S5C. GO analysis of RPS6 target genes revealed that strongly enriched in processes related to RNA splicing and metabolism as well as mitotic cell cycle and helicase activity (Fig. S5D and S5E). AS of RNA is essential for converting genomic instructions into functional proteins, it controls gene expression and protein diversity in many eukaryotes[42]. Subsequently, an investigation was conducted to elucidate the impact of RPS6 on gene and protein expression through its ability to directly target binding and regulate AS. We overlapped the genes from RIP-seq, RNA-seq, proteome and

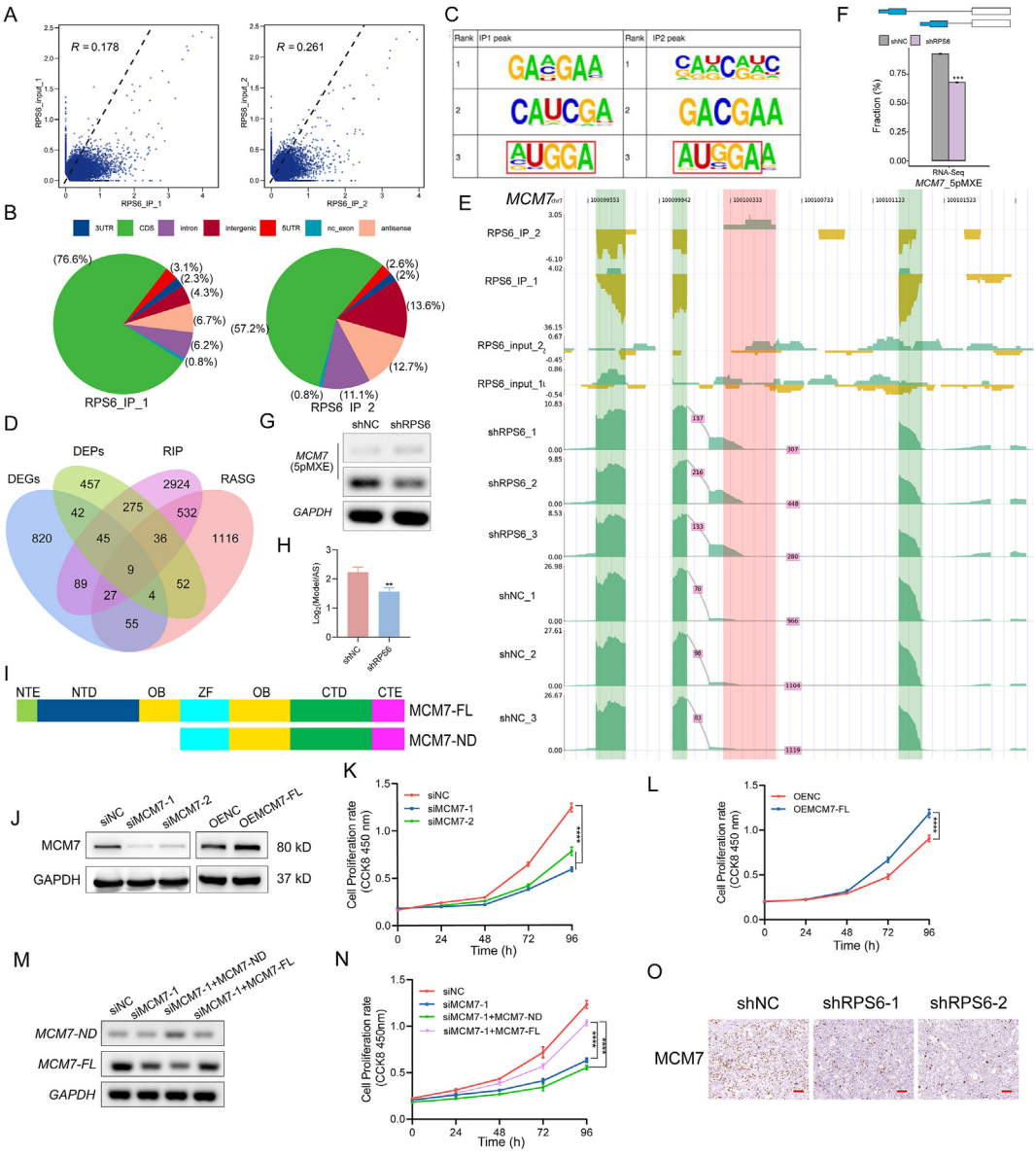

Figure 7 Integrated analysis of RPS6-bound genes and RASE in response to RPS6 knockdown. (A) Correlation analysis of two independent RIP-seq. (B) Pie charts of RPS6-bound peaks across reference genome. (C) Motif enrichment of RPS6-bound peaks by HOMER. (D) Overlap analysis between DEGs, DEPs, RPS6-binding genes and RPS6-RASGs. (E, F) IGV-sashimi plot and RNA-seq quantification of *MCM7* ($n = 3$). (G, H) RT−PCR verify the MXE of *MCM7* in RPS6 knockdown cell ($n = 3$). (I) Schematics showing the main domain of MCM7-FL and MCM7-ND isoform. (J) Western blot was conducted to confirm the expression of MCM7 transfected with siRNA and plasmid. (K, L) CCK-8 assays were performed to determine cell growth after MCM7 was knocked down and overexpressed in RBE cells ($n = 6$). (M) RT-PCR analysis of endogenous and exogenous MCM7 isoforms expression in RBE cells with indicated modifications. (N) Proliferation of RBE cells with indicated modifications ($n = 6$). (O) Representative IHC results and quantification of MCM7 positive staining in xenografted tumors. Scale bar: 50 μm. Data are shown as mean ± SD. $^{**}P < 0.01$; $^{***}P < 0.001$; $^{****}P < 0.0001$.

RASG revealed that nine target genes (Fig. 7D). Among these nine genes, the *MCM7* transcripts had the most RPS6-binding peaks and obviously regulated AS events (Fig. 7E and F). MCM7 is an important member of the MCM family and is involved in DNA helicase enzymes during the S phase of the cell cycle[43]. We then validated the abnormal 5′MXE events of *MCM7* between the RPS6 knockdown and control groups, this AS of *MCM7* produced two different transcripts, which translated two different proteins (named MCM7-FL and MCM7-ND) (Fig. 7G−I), We found that RPS6-KD induced a switch from MCM7-FL to MCM7-ND isoform. Silencing MCM7 with its siRNA significantly inhibited cell growth, while overexpression of MCM7-FL enhanced cell proliferation (Fig. 7J−L). Furthermore, the exogenous MCM7-FL isoform, but not the MCM7-ND isoform, proteins rescued RBE cells growth impaired by siRNA-induced MCM7 silencing (Fig. 7M and N). Moreover, compared with that of the control group, the IHC detection in the xenografted tissues revealed a decreased MCM7 signal after RPS6 knockdown (Fig. 7O). Collectively, these data indicated that MCM7 is a direct target of RPS6, and revealed an isoform-specific function of MCM7 is important for tumor cell growth.

3.9. Targeted RPS6 PMO significantly inhibits the growth of CCA cells and PDOs

We speculated that inhibiting RPS6 might extensively affect CCA growth because it is essential for CCA cell proliferation. To date, a range of treatments, including antibodies and small compounds, have been shown to disrupt the upstream effectors of RPS6[44]. Ribosomes are intricate macromolecular assemblies consisting of a small and large subunit, and RPS6, binds intricately to ribosomal RNA and numerous accessory RPs. Therefore, blocking RPS6 transcription could potentially offer a more effective strategy. To improve the *in vivo* delivery and biodistribution of the blocking nucleotide, we used vivo morpholino, a customized vivo morpholino targeting block for translation initiation was manufactured by Gene Tools LLC, hereafter referred to as RPS6-V-PMO (Fig. 8A). Cell viability assays revealed that RPS6-V-PMO dose-dependently reduced RBE and TFK-1 cell growth compared with NC-V-PMO (Fig. 8B, Fig. S5F). We also observed a weaker inhibitory effect on the viability of HIBEpiC cell (Fig. S5G). PDOs are derived from various patient tumor tissues, have been widely used in tumor pathogenesis research, drug discovery and development, and precision medicine[45]. Next, we investigated the preclinical therapeutic efficacy of RPS6-V-PMO in CCA PDOs, and the growth ability of CCA PDOs were significantly reduced by RPS6-V-PMO (Fig. 8C, Fig. S5H−S5J). And the expression level of RPS6 protein was reduced in RPS6-V-PMO treated RBE cells, it was also shown that the inhibition of RRS6 expression resulted in the increase of p53, p21 and MDM2 (Fig. 8D). Cell cycle analysis indicated that the reduction in RPS6 disrupted cell cycle progression by causing G1 arrest and decreasing the number of cells in S phase (Fig. 8E, Fig. S5K). In addition, EdU staining results also confirmed that inhibition of RPS6 expression *via* RPS6-V-PMO significantly reduced DNA replication activity (Fig. 8F). The efficacy of RPS6-V-PMO treatment *in vivo* was evaluated based on subcutaneous xenograft tumor models of CCA cell, we found that RPS6-V-PMO administration resulted in a significant reduction in tumor volume and mass compared to the control group (Fig. 8G−I). Together, these data demonstrate the preclinical therapeutic efficacy of RPS6-V-PMO treatment in CCA.

4. Discussion

Although management strategies for patients with CCA have improved, the prognosis is still dismal. Identifying the drivers of CCA tumorigenesis is critical for designing potentially targeted medicines. The present study extensively investigated RPS6 and its downstream molecular mechanisms and AS events. We found that the ablation of RPS6 expression induced cell cycle arrest and senescence in CCA cells, by disrupting the AS of gene transcripts such as MCM7. We validated the preclinical therapeutic efficacy of the ASO-mediated translation block of RPS6 *in vivo* and *in vitro*. Collectively, our study demonstrated that RRS6 acts as an oncogenic regulator of CCA development, and it also suggested that RPS6 could be a viable molecular target to impede the progression of CCA.

At the clinical level, RPS6 has been reported to exhibit elevated expression levels in various cancers[16-20], but a full investigation of its relevance to CCA is still lacking. Herein, we found that significantly upregulated RPS6 expression was associated with a shorter OS in patients with CCA. We used loss of RPS6 function experiments to clarify currently unknown details of RPS6 functions in CCA. The results of the cell viability, colony formation, and xenografts in immunocompetent mice showed that RPS6 knockdown reduced cell proliferation and tumorigenicity. Furthermore, RPS6 deficiency induced cell cycle arrest at the G1 phase rather than apoptosis. Cell cycle arrest, which halts the division of cells, is one of the crucial features of cellular senescence[31], and the results confirmed that diminished RPS6 expression induces cellular senescence. These findings indicated that RPS6 may substantially promote CCA cell proliferation, suggesting that RPS6 is a specific and crucial molecule required by CCA cells to maintain infinite proliferative properties and high malignancy.

As an RP, RPS6 plays a crucial role of protein synthesis and has been shown to be associated with cellular growth and survival[14]. To elucidate the downstream profile of the molecular mechanisms of RPS6 in CCA, we conducted comprehensively screened transcriptomes-proteomes from RPS6-defienct CCA cells. We found that RPS6 knockdown reduced the expression of several genes and proteins required for cell cycle progression. Our results confirmed the previous study principle that inhibition of RRS6 led to p53 and p21 accumulation, suppressing the expression of CDKs and cyclins, and leading to cell cycle arrest. These results are consistent with the previous study that depleting RPS6 in A549 cells. A previously study also suggested that the disruption of RPS6 led to the impairment of 40S ribosome synthesis, resulting in a specific elevation in the translation of RPL11, which has binding affinity towards the E3 ubiquitin ligase MDM2[46]. MDM2 is a target of p53, activation of the p53 protein is tightly controlled by its interaction with MDM2, this interaction creates a feedback loop between MDM2 and p53[47,48]. However, we confirmed that the knockdown of RPS6 reduced the expression levels of 40S and 60S ribosomal subunit proteins, which caused a decrease in newly synthesized proteins, and the RPL11 protein levels were also lower in RPS6-shRNA-treated cells than NC cells, indicating that high RPS6 caused p53 accumulation may mediated by the decrease of RPL11 and MDM2. The induction of p53 following ribosomal stress may have a more complicated mechanism, and further investigation is needed to determine the mechanism whereby RP deletion leads to p53 induction.

Intracellular RPs are very abundant proteins, that bind to various RNA molecules and protein complexes outside the ribosome[49].

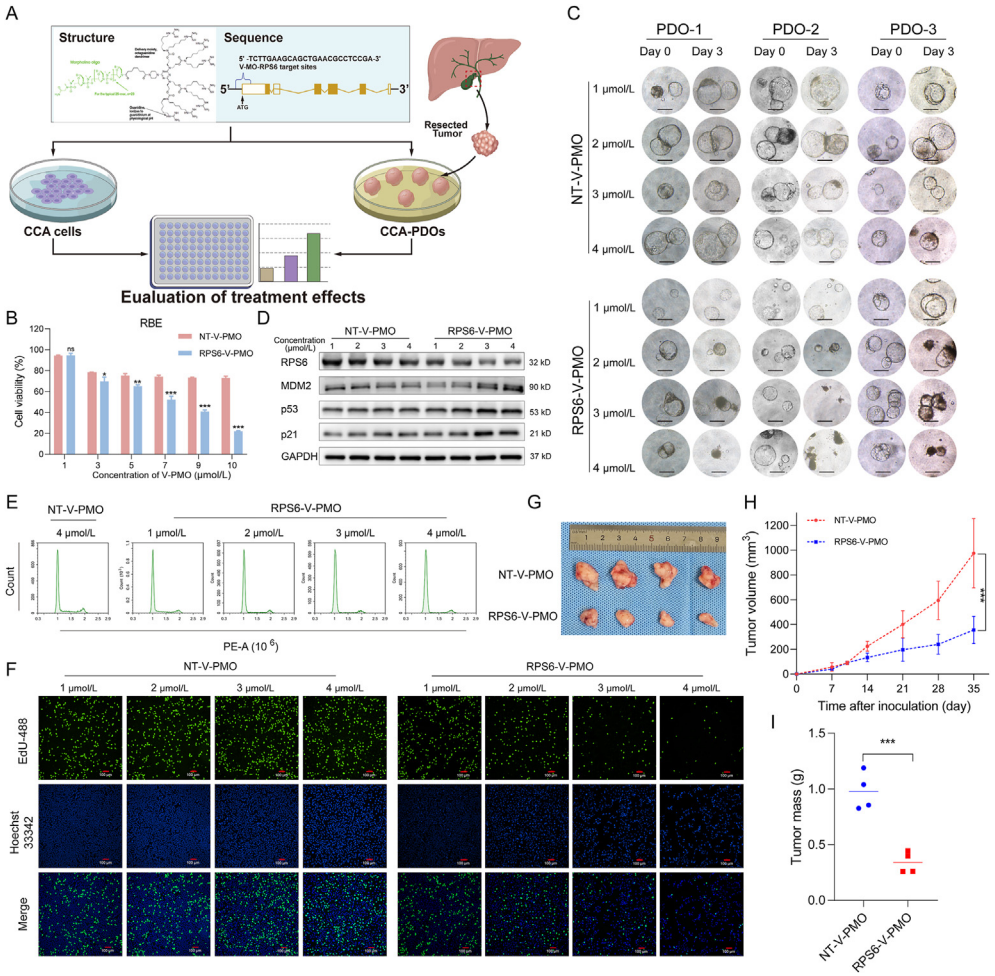

Figure 8 RPS6-V-PMO inhibited CCA cells and PDOs growth. (A) Schematic of the design and efficacy evaluation of RPS6-V-PMO. (B) RPS6-V-PMO inhibit the cell growth of RBE cells ($n = 6$). (C) Representative image of PDOs treated with control or RPS6 PMO. Scale bar: 50 μm. (D) Western blot analysis of RPS6, p53, MDM2 and p21 expression treated with control or RPS6 PMO in RBE cells. (E) FACS image of cell cycle analysis in RBE cells treated with control or RPS6 PMO. (F) EdU assays of RBE cells treated with control or RPS6 PMO. Scale bar: 100 μm. (G–I) The resected subcutaneous tumors from the two groups are depicted in the image, and tumor volumes and mass were calculated ($n = 4$). Data are shown as mean ± SD. ns: not significant; $^{*}P < 0.05$; $^{**}P < 0.01$; $^{***}P < 0.001$.

Many RPs regulate their synthesis by binding to their own transcripts[24,50-54]. Furthermore, RPL22 can cooperate with the AS-related protein heterogeneous nuclear RNP A1, and RPL22 binds to the intronic regions of smad2 pre-mRNA and causes exon 9 skipping[22]. In this study, we identified a splicing network that interacts with RPS6, and demonstrated that loss of RPS6 selectively regulates the AS of certain genes by analysis of RNA-seq data, which has not been previously reported. We investigated the target RNA of RPS6, and the results of previous downstream molecular studies have suggested that an RPS6 deletion mainly affects cell cycle progression. Therefore, we applied a multiomics screening strategy by combining RNA-seq, proteome and RIP-seq, as well as ASEs. We found that RPS6 binds to the *MCM7* mRNA, and silencing of RPS6 significantly inhibits MCM7 mRNA and protein expression levels, AS analysis confirmed that knockdown of RPS6 reduces the ratio of MXE events in MCM7. this ASE leads to different transcript variants, resulting in changes in the functional properties of the translated MCM7 protein. MCM7 is an important member of the MCM family and is considered the authorizing component and checkpoint site of S phase in the cell cycle. For a period after the onset of DNA synthesis, the MCM complex binds to the chromosome and exhibits weak helicase activity under the action of MCM7, whereas the MCM complex breaks away from the chromosome during the G2 phase, indicating the completion of DNA replication[43,55]. Conversely, when RPS6 was knocked down, the alternative transcript isoform MCM7-NTD was translated into a protein lacking 176 amino acids compared to MCM7-FL. Specifically, MCM7-NTD lacks the N-terminal domain (NTD) and the oligonucleotide/oligosaccharide-binding domain, with particular emphasis on the NTD domain, which plays a crucial role in the formation of the MCM complex and the Cdt1–MCM complex[56]. MCM7 has been implicated in the development and progression of tumors and is being evaluated as a possible biomarker in numerous cancers[57-60]. Nevertheless, our work focused on elucidating a new downstream mechanism of RPS6 as an RBP outside ribosome. More investigations are required to fully elucidate the intricate

process underlying the regulation of DNA replication by different transcripts of MCM7.

Small-molecule inhibitors serve as the initial constituents of molecularly targeted medicines in cancer therapy, and have considerable potential to improve the clinical outcomes of patients[61,62]. However, small-molecule inhibitors are less specific and can target more than one molecule[63]. Oligonucleotide therapies represent an evolving type of pharmaceutical intervention encompassing both modified and unmodified short nucleic acid molecules[64,65]. The mechanism of action of oligonucleotide therapy is primarily mediated through pairing of target mRNA, resulting in gene silencing, steric blockade or changes in splicing patterns[66]. In this study, we used *in vivo* PMOs to attenuate RPS6 translation, which significantly inhibited the growth of CCA cells and PDOs. PMOs are composed of short chains consisting of approximately 25 morpholino subunits. Morpholinos function *via* a steric blocking mechanism that operates independently of RNase H and does not result in the degradation of its RNA targets, and they are cell-stable and are not cleaved by nucleases[67]. A Vivo-Morpholino is comprised of morpholino oligo covalently linked to delivery peptides synthesized from octaguanidine dendrimer, while guanidino-delivered peptide is effective penetrating cell membranes, and further increases the stability of the morpholino oligo due to its arginine-rich active ingredient[68]. The FDA has approved several morpholino oligonucleotides[69,70]. The potential of oligonucleotide therapies as cancer treatments has been extensively studied for several decades, demonstrating encouraging results in preclinical and clinical trials[71,72]. Therefore, oligonucleotide therapeutics exploit their specific high-affinity binding to target abnormally expressed or spliced genes that drive tumor development and progression. This provides a promising new approach for the treatment of cancer, especially for the types that lack of targeted drugs. Therefore, we believe that RPS6-related PMOs may be an effective strategy for CCA treatment.

The limitation of our study is the small sample size for proteomics analysis of CCA tissue samples. We acknowledge the potential impact of this limitation on the comprehensiveness of our findings. Furthermore, we did not extensively explore the interaction between RPS6 and SF3B1, and how this interaction triggers the AS of *MCM7*. Previous studies have indeed demonstrated that the function of SF3B1 can lead to AS of *MCM7*, resulting in the utilization of different exons[73]. Future studies focusing on investigations into specific protein interactions are warranted to deepen our understanding of the oncogenic mechanisms of RPS6 in CCA.

5. Conclusions

In conclusion, our studies utilizing clinical samples from CCA patients, PDOs and CCA cell lines have shown that targeting RPS6 inhibits cancer progression. The mechanisms involving the cell cycle are related to MCM7-mediated DNA replication, extending beyond its traditional role in protein synthesis. These results suggest that targeting RPS6 for the treatment of CCA is a compelling approach. In addition, vivo morpholinos represent a promising therapeutic strategy.

Acknowledgments

This work was supported by the National Key Research and Development Program of China (2022YFC2407405); National Natural Science Foundation of China (82060551, 32160230); Natural Science foundation of Gansu Province (22JR5RA891, China); Gansu Provincial Health Industry Research Program (GSWSQH2021-001, China); Science and Technology Bureau Talent Innovation Program of Chengguan District (2019RCCX0038, China).

Author contributions

Wenkang Fu: Writing − review & editing, Writing − original draft, Formal analysis, Data curation, Conceptualization. Yanyan Lin: Writing − review & editing, Writing − original draft, Methodology, Investigation. Mingzhen Bai: Writing − original draft, Software, Formal analysis, Conceptualization. Jia Yao: Writing − review & editing, Supervision, Project administration, Investigation, Funding acquisition, Conceptualization. Chongfei Huang: Validation, Software, Data curation. Long Gao: Visualization, Investigation, Formal analysis. Ningning Mi: Methodology, Formal analysis, Conceptualization. Haidong Ma: Validation, Software, Data curation. Liang Tian: Visualization, Software, Data curation. Ping Yue: Conceptualization, Resources. Yong Zhang: Investigation, Resources. Jinduo zhang: Validation, Project administration, Methodology. Yanxian Ren: Writing − review & editing, Methodology, Formal analysis. Liyun Ding: Supervision, Methodology, Conceptualization. Lunzhi Dai: Software, Investigation. Joseph W. Leung: Writing − review & editing, Supervision. Jinqiu Yuan: Writing − review & editing, Visualization, Supervision, Methodology. Wenhua Zhang: Writing − review & editing, Writing − original draft, Supervision, Conceptualization. Wenbo Meng: Writing − review & editing, Writing − original draft, Supervision, Resources, Methodology, Conceptualization.

Conflicts of interest

The authors declare no conflicts of interest.

Appendix A. Supporting information

Supporting information to this article can be found online at https://doi.org/10.1016/j.apsb.2024.06.028.

References

1. Brindley PJ, Bachini M, Ilyas SI, Khan SA, Loukas A, Sirica AE, et al. Cholangiocarcinoma. *Nat Rev Dis Primers* 2021;**7**:65.
2. Banales JM, Cardinale V, Carpino G, Marzioni M, Andersen JB, Invernizzi P, et al. Expert consensus document: cholangiocarcinoma: current knowledge and future perspectives consensus statement from the European Network for the Study of Cholangiocarcinoma (ENS-CCA). *Nat Rev Gastroenterol Hepatol* 2016;**13**:261−80.
3. Jarnagin WR, Fong Y, DeMatteo RP, Gonen M, Burke EC, Bodniewicz BJ, et al. Staging, resectability, and outcome in 225 patients with hilar cholangiocarcinoma. *Ann Surg* 2001;**234**:507−19.
4. van Vugt JLA, Gaspersz MP, Coelen RJS, Vugts J, Labeur TA, de Jonge J, et al. The prognostic value of portal vein and hepatic artery involvement in patients with perihilar cholangiocarcinoma. *HPB Oxf* 2018;**20**:83−92.
5. Sharifi-Noghabi H, Zolotareva O, Collins CC, Ester M. MOLI: multi-omics late integration with deep neural networks for drug response prediction. *Bioinformatics* 2019;**35**:i501−9.
6. Clark DJ, Dhanasekaran SM, Petralia F, Pan J, Song X, Hu Y, et al. Integrated proteogenomic characterization of clear cell renal cell carcinoma. *Cell* 2019;**179**:964−3.e31.

7. Dou Y, Kawaler EA, Cui Zhou D, Gritsenko MA, Huang C, Blumenberg L, et al. Proteogenomic characterization of endometrial carcinoma. *Cell* 2020;**180**:729−8.e26.
8. Gao Q, Zhu H, Dong L, Shi W, Chen R, Song Z, et al. Integrated proteogenomic characterization of HBV-related hepatocellular carcinoma. *Cell* 2019;**179**:1240.
9. Jiang Y, Sun A, Zhao Y, Ying W, Sun H, Yang X, et al. Proteomics identifies new therapeutic targets of early-stage hepatocellular carcinoma. *Nature* 2019;**567**:257−61.
10. Li C, Sun YD, Yu GY, Cui JR, Lou Z, Zhang H, et al. Integrated omics of metastatic colorectal cancer. *Cancer Cell* 2020;**38**:734−7.e9.
11. Vasaikar S, Huang C, Wang X, Petyuk VA, Savage SR, Wen B, et al. Proteogenomic analysis of human colon cancer reveals new therapeutic opportunities. *Cell* 2019;**177**:1035−49.e19.
12. Meyuhas O. Physiological roles of ribosomal protein S6: one of its kind. *Int Rev Cell Mol Biol* 2008;**268**:1−37.
13. Hirashita T, Hirashita Y, Iwashita Y, Endo Y, Kiyonaga M, Matsumoto S, et al. S6 ribosomal protein phosphorylation is associated with malignancy of intraductal papillary mucinous neoplasm of the pancreas. *Ann Gastroenterol Surg* 2020;**4**:571−9.
14. Ruvinsky I, Meyuhas O. Ribosomal protein S6 phosphorylation: from protein synthesis to cell size. *Trends Biochem Sci* 2006;**31**:342−8.
15. Warner JR, McIntosh KB. How common are extraribosomal functions of ribosomal proteins?. *Mol Cell* 2009;**34**:3−11.
16. Yang X, Xu L, Yang YE, Xiong C, Yu J, Wang Y, et al. Knockdown of ribosomal protein S6 suppresses proliferation, migration, and invasion in epithelial ovarian cancer. *J Ovarian Res* 2020;**13**:100.
17. Chen B, Zhang W, Gao J, Chen H, Jiang L, Liu D, et al. Down-regulation of ribosomal protein S6 inhibits the growth of non-small cell lung cancer by inducing cell cycle arrest, rather than apoptosis. *Cancer Lett* 2014;**354**:378−89.
18. Chaisuparat R, Rojanawatsirivej S, Yodsanga S. Ribosomal protein S6 phosphorylation is associated with epithelial dysplasia and squamous cell carcinoma of the oral cavity. *Pathol Oncol Res* 2013;**19**:189−93.
19. Zheng Z, Zheng Y, Zhang M, Wang J, Yu G, Fang W. Reciprocal expression of p-AMPKa and p-S6 is strongly associated with the prognosis of gastric cancer. *Tumour Biol* 2016;**37**:4803−11.
20. Yanai A, Inoue N, Yagi T, Nishimukai A, Miyagawa Y, Murase K, et al. Activation of mTOR/S6K but not MAPK pathways might be associated with high Ki-67, ER^+, and $HER2^-$ breast cancer. *Clin Breast Cancer* 2015;**15**:197−203.
21. Liu Y, Deisenroth C, Zhang Y. RP−MDM2−p53 pathway: linking ribosomal biogenesis and tumor surveillance. *Trends Cancer* 2016;**2**:191−204.
22. Zhang Y, O'Leary MN, Peri S, Wang M, Zha J, Melov S, et al. Ribosomal proteins Rpl22 and Rpl22l1 control morphogenesis by regulating pre-mRNA splicing. *Cell Rep* 2017;**18**:545−56.
23. Vilardell J, Warner JR. Ribosomal protein L32 of *Saccharomyces cerevisiae* influences both the splicing of its own transcript and the processing of rRNA. *Mol Cell Biol* 1997;**17**:1959−65.
24. Malygin AA, Parakhnevitch NM, Ivanov AV, Eperon IC, Karpova GG. Human ribosomal protein S13 regulates expression of its own gene at the splicing step by a feedback mechanism. *Nucleic Acids Res* 2007;**35**:6414−23.
25. Licatalosi DD, Darnell RB. RNA processing and its regulation: global insights into biological networks. *Nat Rev Genet* 2010;**11**:75−87.
26. Ramakrishnan V, White SW. Ribosomal protein structures: insights into the architecture, machinery and evolution of the ribosome. *Trends Biochem Sci* 1998;**23**:208−12.
27. Qi S, Guo L, Yan S, Lee RJ, Yu S, Chen S. Hypocrellin A-based photodynamic action induces apoptosis in A549 cells through ROS-mediated mitochondrial signaling pathway. *Acta Pharm Sin B* 2019;**9**:279−93.
28. Ravi V, Jain A, Mishra S, Sundaresan NR. Measuring protein synthesis in cultured cells and mouse tissues using the non-radioactive SUnSET assay. *Curr Protoc Mol Biol* 2020;**133**:e127.
29. Alabi A, Xia XD, Gu HM, Wang F, Deng SJ, Yang N, et al. Membrane type 1 matrix metalloproteinase promotes LDL receptor shedding and accelerates the development of atherosclerosis. *Nat Commun* 2021;**12**:1889.
30. Hart T, Chandrashekhar M, Aregger M, Steinhart Z, Brown KR, MacLeod G, et al. High-resolution CRISPR screens reveal fitness genes and genotype-specific cancer liabilities. *Cell* 2015;**163**:1515−26.
31. Kumari R, Jat P. Mechanisms of cellular senescence: cell cycle arrest and senescence associated secretory phenotype. *Front Cell Dev Biol* 2021;**9**:645593.
32. Magnuson B, Ekim B, Fingar DC. Regulation and function of ribosomal protein S6 kinase (S6K) within mTOR signalling networks. *Biochem J* 2012;**441**:1−21.
33. Bursac S, Brdovcak MC, Donati G, Volarevic S. Activation of the tumor suppressor p53 upon impairment of ribosome biogenesis. *Biochim Biophys Acta* 2014;**1842**:817−30.
34. Chen J. The cell-cycle arrest and apoptotic functions of p53 in tumor initiation and progression. *Cold Spring Harb Perspect Med* 2016;**6**:a026104.
35. Li K, You J, Wu Q, Meng W, He Q, Yang B, et al. Cyclin-dependent kinases-based synthetic lethality: evidence, concept, and strategy. *Acta Pharm Sin B* 2021;**11**:2738−48.
36. Bochman ML, Schwacha A. The Mcm complex: unwinding the mechanism of a replicative helicase. *Microbiol Mol Biol Rev* 2009;**73**:652−83.
37. Li D, Yu W, Lai M. Towards understandings of serine/arginine-rich splicing factors. *Acta Pharm Sin B* 2023;**13**:3181−207.
38. Kim D, Pertea G, Trapnell C, Pimentel H, Kelley R, Salzberg SL. TopHat2: accurate alignment of transcriptomes in the presence of insertions, deletions and gene fusions. *Genome Biol* 2013;**14**:R36.
39. Jin L, Li G, Yu D, Huang W, Cheng C, Liao S, et al. Transcriptome analysis reveals the complexity of alternative splicing regulation in the fungus *Verticillium dahliae*. *BMC Genomics* 2017;**18**:130.
40. Gerstberger S, Hafner M, Tuschl T. A census of human RNA-binding proteins. *Nat Rev Genet* 2014;**15**:829−45.
41. Draper DE, Reynaldo LP. RNA binding strategies of ribosomal proteins. *Nucleic Acids Res* 1999;**27**:381−8.
42. Marasco LE, Kornblihtt AR. The physiology of alternative splicing. *Nat Rev Mol Cell Biol* 2023;**24**:242−54.
43. Wang Y, Chen H, Zhang J, Cheng ASL, Yu J, To KF, et al. MCM family in gastrointestinal cancer and other malignancies: from functional characterization to clinical implication. *Biochim Biophys Acta Rev Cancer* 2020;**1874**:188415.
44. Yi YW, You KS, Park JS, Lee SG, Seong YS. Ribosomal protein S6: a potential therapeutic target against cancer?. *Int J Mol Sci* 2021;**23**:48.
45. Veninga V, Voest EE. Tumor organoids: opportunities and challenges to guide precision medicine. *Cancer Cell* 2021;**39**:1190−201.
46. Fumagalli S, Di Cara A, Neb-Gulati A, Natt F, Schwemberger S, Hall J, et al. Absence of nucleolar disruption after impairment of 40S ribosome biogenesis reveals an rpL11-translation-dependent mechanism of p53 induction. *Nat Cell Biol* 2009;**11**:501−8.
47. Moll UM, Petrenko O. The MDM2−p53 interaction. *Mol Cancer Res* 2003;**1**:1001−8.
48. Feng Y, Han Y, Hu A, Qu Y, Hu Y, Wu H, et al. Heliangin acts as a covalent ligand of RPS2 that disrupts pre-rRNA metabolic processes in NPM1-mutated acute myeloid leukemia. *Acta Pharm Sin B* 2023;**13**:598−617.
49. Xue S, Barna M. Specialized ribosomes: a new frontier in gene regulation and organismal biology. *Nat Rev Mol Cell Biol* 2012;**13**:355−69.
50. Eng FJ, Warner JR. Structural basis for the regulation of splicing of a yeast messenger RNA. *Cell* 1991;**65**:797−804.
51. Fewell SW, Woolford Jr JL. Ribosomal protein S14 of *Saccharomyces cerevisiae* regulates its expression by binding to RPS14B pre-mRNA and to 18S rRNA. *Mol Cell Biol* 1999;**19**:826−34.
52. Badis G, Saveanu C, Fromont-Racine M, Jacquier A. Targeted mRNA degradation by deadenylation-independent decapping. *Mol Cell* 2004;**15**:5−15.
53. Mitrovich QM, Anderson P. Unproductively spliced ribosomal protein mRNAs are natural targets of mRNA surveillance in *C. elegans*. *Genes Dev* 2000;**14**:2173−84.

54. O'Leary MN, Schreiber KH, Zhang Y, Duc AC, Rao S, Hale JS, et al. The ribosomal protein Rpl22 controls ribosome composition by directly repressing expression of its own paralog, Rpl22l1. *Plos Genet* 2013;**9**:e1003708.
55. Laskey RA, Madine MA. A rotary pumping model for helicase function of MCM proteins at a distance from replication forks. *EMBO Rep* 2003;**4**:26−30.
56. Zhai Y, Li N, Jiang H, Huang X, Gao N, Tye BK. Unique roles of the non-identical MCM subunits in DNA replication licensing. *Mol Cell* 2017;**67**:168−79.
57. Ren B, Yu G, Tseng GC, Cieply K, Gavel T, Nelson J, et al. MCM7 amplification and overexpression are associated with prostate cancer progression. *Oncogene* 2006;**25**:1090−8.
58. Toyokawa G, Masuda K, Daigo Y, Cho HS, Yoshimatsu M, Takawa M, et al. Minichromosome maintenance protein 7 is a potential therapeutic target in human cancer and a novel prognostic marker of non-small cell lung cancer. *Mol Cancer* 2011;**10**:65.
59. Zhou YM, Zhang XF, Cao L, Li B, Sui CJ, Li YM, et al. MCM7 expression predicts post-operative prognosis for hepatocellular carcinoma. *Liver Int* 2012;**32**:1505−9.
60. Facoetti A, Ranza E, Grecchi I, Benericetti E, Ceroni M, Morbini P, et al. Immunohistochemical evaluation of minichromosome maintenance protein 7 in astrocytoma grading. *Anticancer Res* 2006;**26**:3513−6.
61. Imai K, Takaoka A. Comparing antibody and small-molecule therapies for cancer. *Nat Rev Cancer* 2006;**6**:714−27.
62. Wu D, Li Y, Zheng L, Xiao H, Ouyang L, Wang G, et al. Small molecules targeting protein−protein interactions for cancer therapy. *Acta Pharm Sin B* 2023;**13**:4060−88.
63. Gerber DE. Targeted therapies: a new generation of cancer treatments. *Am Fam Physician* 2008;**77**:311−9.
64. Mehta M, Deeksha, Tewari D, Gupta G, Awasthi R, Singh H, et al. Oligonucleotide therapy: an emerging focus area for drug delivery in chronic inflammatory respiratory diseases. *Chem Biol Interact* 2019;**308**:206−15.
65. Gao K, Huang L. Achieving efficient RNAi therapy: progress and challenges. *Acta Pharm Sin B* 2013;**3**:213−25.
66. Crooke ST, Baker BF, Crooke RM, Liang XH. Antisense technology: an overview and prospectus. *Nat Rev Drug Discov* 2021;**20**:427−53.
67. Egli M, Manoharan M. Chemistry, structure and function of approved oligonucleotide therapeutics. *Nucleic Acids Res* 2023;**51**:2529−73.
68. Morcos PA, Li Y, Jiang S. Vivo-Morpholinos: a non-peptide transporter delivers morpholinos into a wide array of mouse tissues. *Biotechniques* 2008;**45**:613−4. 6, 8 passim.
69. Aartsma-Rus A, Corey DR. The 10th oligonucleotide therapy approved: golodirsen for Duchenne muscular dystrophy. *Nucleic Acid Ther* 2020;**30**:67−70.
70. Shirley M. Casimersen: first approval. *Drugs* 2021;**81**:875−9.
71. Wan J, Bauman JA, Graziewicz MA, Sazani P, Kole R. Oligonucleotide therapeutics in cancer. *Cancer Treat Res* 2013;**158**:213−33.
72. Xiong H, Veedu RN, Diermeier SD. Recent advances in oligonucleotide therapeutics in oncology. *Int J Mol Sci* 2021;**22**:3295.
73. Dolatshad H, Pellagatti A, Fernandez-Mercado M, Yip BH, Malcovati L, Attwood M, et al. Disruption of SF3B1 results in deregulated expression and splicing of key genes and pathways in myelodysplastic syndrome hematopoietic stem and progenitor cells. *Leukemia* 2015;**29**:1092−103.